POLITECNICO DI TORINO

Corso di Laurea Magistrale in Ingegneria Aerospaziale

Numerical investigation of forced response in the bladed disks with frictional damping in blade root section

---

Supervisors

Prof. Daniele Botto

Dr. Egor A. Garshin

Candidate

Nicolas Olivo

July 2020

Acknowledgements

I would like to thank my entire family for the support and motivation given those years. Especially my parents Mauro and Michela for the psychological and financial support needed day by day and to be my reference point. My brother Iacopo for the academic inspiration and to allow me to discover the fantastic city of Turin.
My sincere gratitude to my supervisors Prof. Daniele Botto and Egor A. Garshin for the support during the thesis writing. A special thank to Prof. Alexander Vinogradov, from the Samara University, that took care of me and my friends, Guido and Antonino, during the memorable time spent in Samara.
I would like to thank my friends form Aegee Samara to be my guide and reference point in Russia in addition to Beatrice and Adriana for the time spent together in Samara. My sincere gratitude to my girlfriend Sara for the support and for the closeness in difficult moments. I would like to thank Marco, Enrico, Stefano, Matteo and another time my parents for the job motivation.
I would like to thank all my friends from Aesa, Simone and colleagues from Polytechnic of Turin and University of Padova for the moments spent together in the classes, libraries and in the cities. My sincere gratitude to the ACMDF team to be my group of friends and for the support in difficult moments.
I sincerely wish a great health, a good family and professional success to all the people mentioned above and to all the honest people that i know as well as a life full of desire to discover the world.

Contents

Abstract

The stress produced by vibration is a common and well investigated problem in the word of aviation. The stress caused by vibration can drastically reduce the life of a turbine engine and one of the main affected part of the engine are the blades. Design a last generation of gas turbine engine focusing on its reliability is a complicated task that can present a lot of problems.

The solution of this task overall different problems such as:

1. low-cycle and high-cycle fatigue
2. resonance frequencies
3. corrosion of blades
4. etc.

The blade has to be connected to the disk and before provide this assembly the dynamic behaviour must be predicted using different calculation methods available. The Finite Element Method (FEM) is one of the numerical methods that can solve the engineer calculation and and more precise than the analytical one.

The damping evolved in contact surfaces between the root blade and the disk perform a fundamental rule in the dynamic analysis of a bladed disk and predict how it change the dynamic behaviour of the system is one of the task requested during the design of the disk assembly.

A numerical model based on the contact mechanics principles is performed and using a finite element modelling software is possible to use that theory and evaluate a result. This procedure allow to quantify the damping generated at the contact of the root blade and the disk for different friction coefficients.

The model evaluated in [2] is inserted in the modal analysis of the system and both numerical and experimental results are compared on order to confirm the results produced by the numerical investigation.

1 Introduction

1.1 General knowledge

Improving the life-time and the reliability of aircraft turbine engine is one of the major task during the design process of an engine. beside this main task there are some other advantages that we must take in account such as: reducing the cost and the number of engine maintenance, increase the economy of the airplane because the number of engine decrease, reducing of aircraft stand idles.
In order to successful design an engine solving other problems connected to the time of work is required. Anyway the traditional strength issues had to be fixed. The main problems correlated to the time of work are:

1. long-term strength, creep and stress relaxation in details during long work in steady-state conditions
2. repeatedly-static fatigue and thermo-cyclic strength connected with large number of starts, stops and changing of engine operation mode during engine life-time
3. high-cycle fatigue, especially for high-temperature-resistant and non-ferrous alloys, for which it reduces continuously during its work
4. changing of surface from corrosion and erosion
5. wear and fretting-wear in contact pairs

One of the major cause of deteriorate gas turbine engine is the high-cycle fatigue and inspect the vibration loads in the design process can increase the life of the engine [28] and investigate the the contact of the root blade and the disk can help to decrease those type of vibrations.
Is clear that one of the major task of design a gas turbine engine is reduce the level of vibration and for achieve this objective is important to study the structural and dynamic of the blades. The dynamic characteristics includes their natural frequencies and how is possible to provide damping for various mode of vibration.

Mechanical wear The region identified as the contact between the root section and the disc can be affected by mechanical wear because the friction between those areas is useful to control the dynamic behaviour of the system. The main disadvantages of the mechanical wearing are the separation of small pieces of metal after the cyclic elastic and plastic deformation. Those stress is a dangerous stress concentrator and fractures in the surface layer can appear as well as increasing the wear. Concerning the mechanical wear hard alloys can reduce this problem.

Aerodynamic damping The damping of vibration in a blade is generally made by the aerodynamic damping and the non-aerodynamic sources. The aerodynamic damping is straightly correlated with the CFD study of the blade [1]. Is possible to study how the flow impact on the blade and the aim is to obtain the profile of the blade that minimize the vibration produced by the flow. One of the major problems in aerodynamic vibration is the flutter and in order to provide a good result of the simulation the profile of the blade, cascade of the stages, angle of incidence and the condition of the flow, intended as subsonic, transonic or supersonic, should be taken in account.

Material damping As is described in [12] the material damping is a name for the complex physical effects that convert kinetic and strain energy in a vibrating mechanical system consisting in a volume of macro continuous matter into heat. When a material is under cyclic stress mechanism such plastic slip, dislocation etc. are involved. Those mechanisms permit the creation of the hysteresis loop diagram illustrated in the figure 6 and the energy dissipated during one cycle is the area included in the hysteresis diagram. In the recent generation of gas turbine engine titanium-based and nickel-based alloys are involved during the manufacturing project of the blades. As reported in [2] is possible to neglect the material damping of those materials because it does not have a notable value. Is possible to obtain various values of material damping consulting [26] and for a fan blade of titanium the material damping coefficient is nearby 0.00003 for the first and second bending mode and for the torsion mode is almost negligible because the coefficient is 0.0001.
For high frequencies is demonstrated that the structural damping is almost negligible and the dissipation of damping take place due the energy dissipation in the material. For this reason during the design procedure of the gas turbine engine is important to take in account that the coatings can be used as a dumper as well as visco-elastic material patches that can be inserted into the cavities of the elements due increasing damping.

Friction damping The friction damping appears when two elements are in contact and the surface between those elements clamp them together. The clamping reaction depends by the external force applied to the system and is not taken in account if the force provide relative motion between two elements or pressure fit, but the force acts in the common interface of the two elements. Considering an external force that gradually increase different conditions takes place in the contact interface depending the force value and how the system can react. At a first sight there are three different situations:

1. The force is enough to produce a shear reaction in the contact region, however the system react as a single elastic body. This condition take place because the share force can not provide slip in the contact region

2. The force increase and the shear reaction in enough to produce relative slip. In some region of the body the shear reaction go over the friction coefficient of common region between the two surfaces and a slight slip appears. This motion condition of microslip in opposite ways of the faces can not interest the complete common area if the shear force is not enough. The mechanical energy involved in the surface is converted into thermal energy and a damping effect take place

3. The force increase and the shear reaction in enough to produce relative slip in the complete contact region. In this condition the shear force is higher and the slip is extended in the entire surface than the microslip becomes gross slip

The motion of the two bodies can be affected from external parameters and the motion condition can change depending the force involved, coefficient of friction, the pressure involved in the surfaces, the normal force applied in the contact region, the roughness of the materials, surface treatments, temperature, frequency of vibration, properties of the materials etc. This condition produces a non linear analysis of the problem and the linearisation of the case of study occur and must be specifically evaluated each time.

Reducing the vibrations Considering a generic mechanical system the vibration can be reduced generally in three ways:

1. damping. This way use a special unit or contact region, like in our case, that can dissipate energy of vibration using friction. In the earlier turbofan engine was common to insert anti-vibration shelves in the fan, but this solution deflect the airflow and part of its energy is lost. In order to create a region where the energy can be dissipated is possible to cut the root of the blade. This anti-vibration solution is possible to be found in some previous generation of ester Europe turbofan engine.

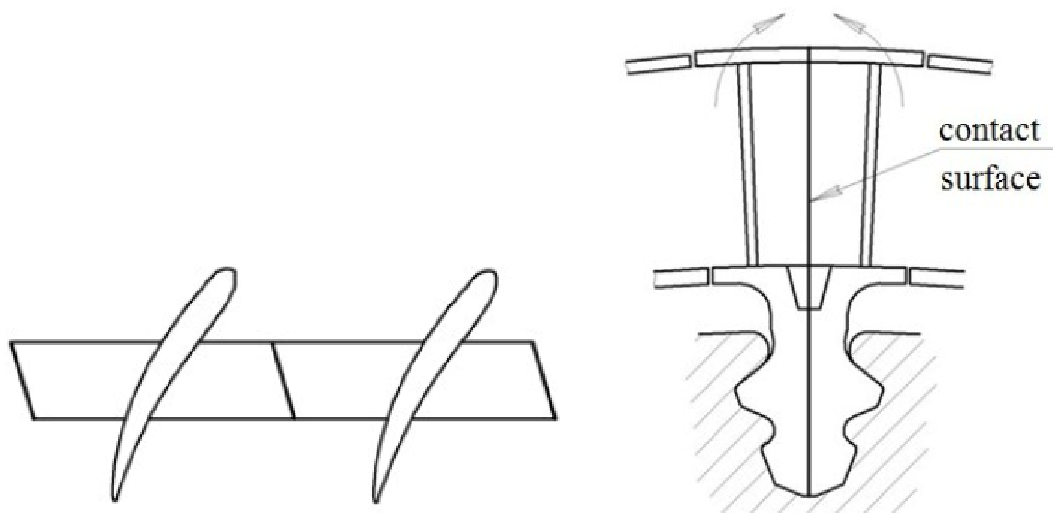

(a) *anti-vibration shelve* (b) *anti-vibration cut root blade*

Figure 1: Examples of anti-vibration solution [28]

2. tune-out of the working frequencies. Basically changing the stiffness of the support will change the position of the critical speed that will move up if stiffness is increased and in the other way if there is a reduction of the stiffness. Due the non-possibility to change the stiffness of the support of the disk the solution is changing its thickness in required positions in order to change the global stiffness of the element. As indicated in the figure 2 the $\Delta\omega$ represent the safety 10% margin of vibration near the critical frequency, however this value can change depending the design choices.

3. reducing of the exciting force. The common way to solve this problem is balancing the rotor adding or removing some little masses, it depends if the unbalanced item is the turbine or the compressor. Another way to solve this problem is to reduce the irregularity of pressure and velocity of the gas flow that impact on the blade. The generally known ways are different. The first way is to increase the radial gap of the stage in order to outdistance the rotor and the stator, however the length and the weight of the engine will be affected of this choice. The second way is to distribute in an irregular way the ribs of the engine in order to produce an unreliable exciting harmonic frequency. Another way could be provide an inclined distributor for example.

Vibration mode shape Assuming a blade with two degrees of freedom that are displacement and turn angle and an extremely rigid fastening the own frequencies of the blade

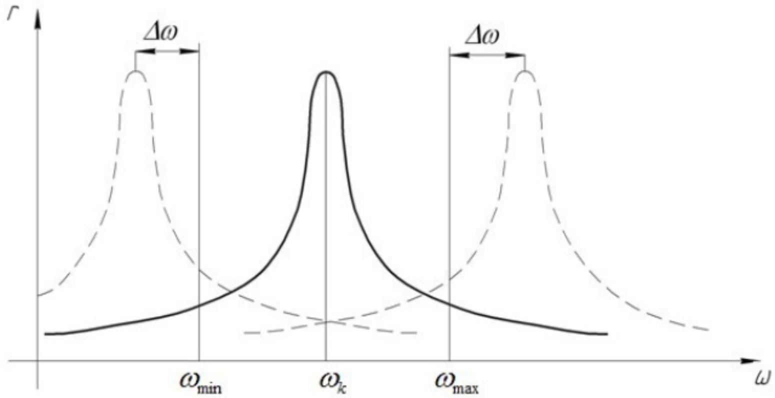

Figure 2: Generic tune-out of frequency [28]

are [28]:

$$p_i = \left(\frac{K_i{}^2}{l}\right)\sqrt{\frac{EJ_y}{\rho F}} \tag{1}$$

Depending the values of Ki this equation shows that the blade have different own frequencies and every one has only one mode shape. In the figure 3 are represented the first three mode shape related to the bending of the blade, but every blade has a never-ending number of mode.

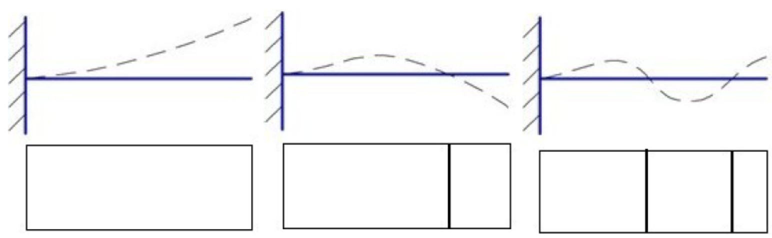

Figure 3: First, second and third mode shape for bending [28]

Considering a 2D blade and considering only the mode shape described in the equation 1 is possible to derive different frequencies: $f_{1x1} < f_{2x1} < f_{3x1} < \ldots$, as illustrated in the figure3.
Considering the equation 1 another important parameter are the consequences of the material properties detailed in $\sqrt{\frac{E}{\rho}}$. Is possible to ensure that if the Young modulus increase also p_i increase and adjust those values during the design process is useful to control the value of a critical frequency.
Following the theory described in [28] considering a disk as a Timoshenko plate with non-constant thickness is possible to determine the equilibrium using a cylindrical coordinate system $\tilde{M}_r, \tilde{Q}_r, \tilde{M}_{r\varphi}, \tilde{M}_\varphi, \tilde{Q}_\varphi$.
The mode shape of the disk are describes using the m and n parameters where the first identify the net diameters and the second the net circles. if $n = 1$ there will be one point along the radius where the amplitude of the vibration is equal zero. Following this law if $n > 0$ and $m = 0$ the mode shape of the vibration of the disk present present one or multiple points, depends on the value of n, where the amplitude of the vibration is zero. That particular mode shape is called umbrella shape.

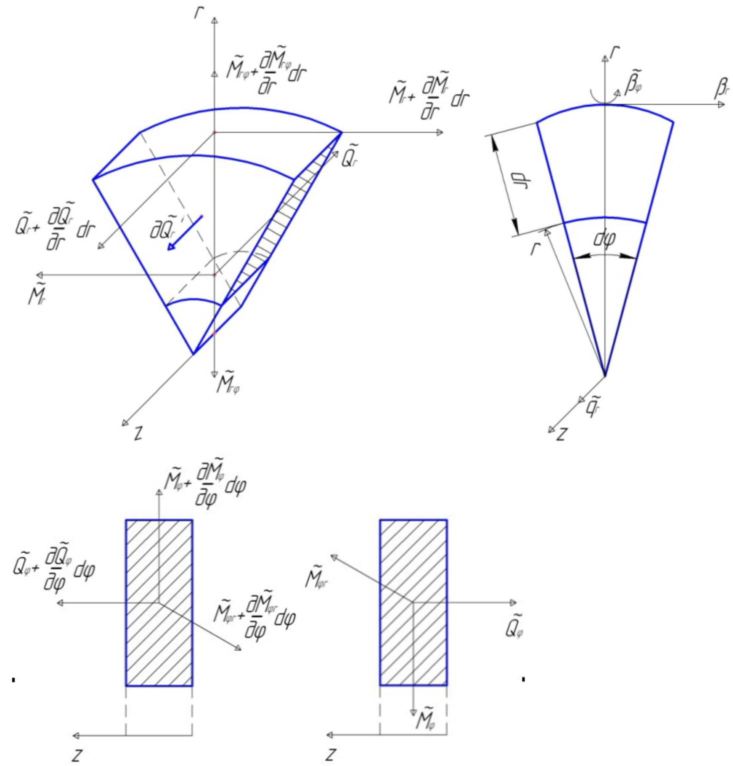

Figure 4: Forced in an infinite element of disk [28]

Is possible to obtain different modes of shape of the disk as presented in the figure 5 and is possible to notice an increase of the own frequency of the disk if m and n values increase. Combining the blade and the disk is possible to notice that the own frequency of the system decrease as a result of adding mass in the peripheral section of the disk.

Hysteresis diagram In a generic elasto-plastic body deformation take place when it is loaded. Every body has an a potential energy of deformation indicated with Π in the figure 6 and can be assumed as the area under the elastic deformation line. The elastic deformation of the body evolves the displacement δ of the generic point in the body and its reaction load P that does not represent the load.
The load P_{tot} can be described, for a first approximation as the $P_{elastic} + P_{friction}$ and for the unload is minus the $P_{friction}$. Is understandable that if $P_{friction}$ increase the potential energy of deformation of the generic body increase too so the hysteresis loop area $\Delta\Pi$ raise. The area of the loading-unloading cycle is defined as the energy dissipated among the load and unload loads, or simply the cycle.
Is it possible to take in account the energy dissipation coefficient $\psi = \frac{\Delta\Pi}{\Pi}$ that represent the ratio between the two areas involved. ψ is a property of the mechanical system and depends from the exciting force ω_k and the stiffness of the system C_k, therefore $\psi = \frac{2\pi b_k \omega_k}{C_k}$ [28].

$$m\frac{d^2\delta_k}{dt^2} + b_k\frac{d\delta_k}{dt} + C_k\delta_k = F_k \sin \omega_k t \tag{2}$$

Considering a system with a force excitation vibration in the k axis is possible to obtain a

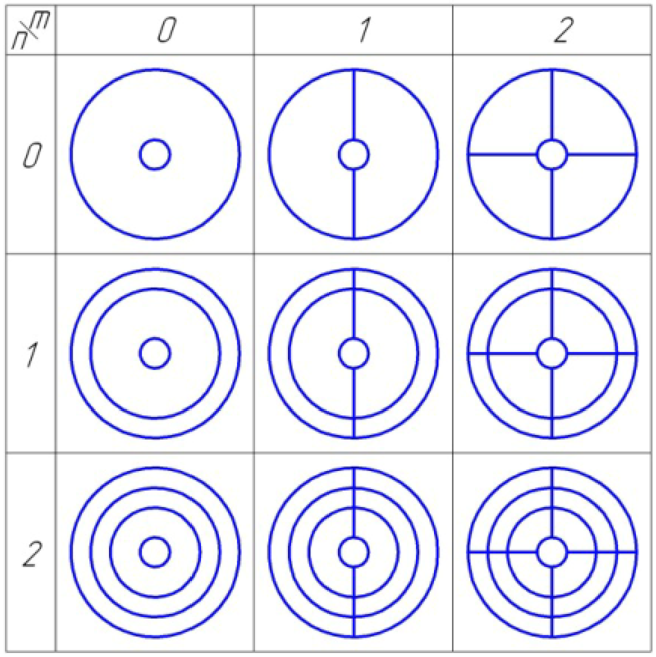

Figure 5: Mode shape of the disk combining m and n [28]

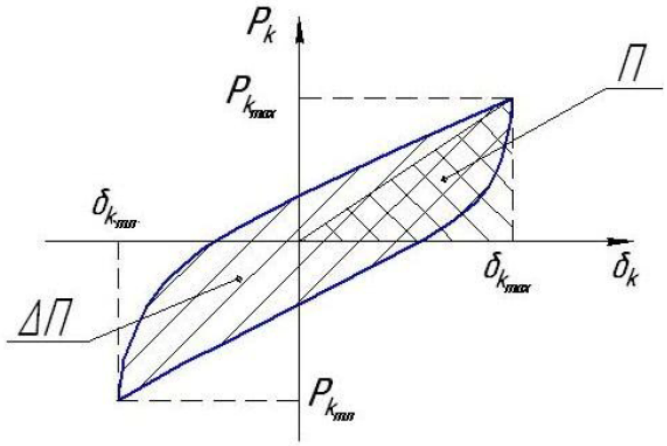

Figure 6: Hysteric cycle of deformation [28]

differential equation 2 that describe the motion of the system.
Is it possible to describe the coefficient γ_k as the value that connects the two elements of a mechanic system: the force applied and its motion. If the system can be described as a linear one the shape of the hysteresis loop can be showed as an ellipsis shape, therefore if the system is not linear the hysteresis loop has another shape. In the case of contact between the root of the blade and the disk the system is not linear.

1.2 State of art

The couple blade plus disk is vastly investigated and a lot of publications focusing in the failure of the attachment of those two important elements of a gas turbine engine. The major failure investigation is correlated to the fretting phenomenons that causes crack in the root of the blade for example. Papers have also investigated the stress and the strain distribution in the connection blade-disk regions as in the joint interfaces and on critical condition for creep formation.
In this paper the stress and the energy dissipation of the contact region for each cycle is calculated and is possible to predict the strain and the strain in the contact regions due the blade vibration. Is proved by [2] and [24] that usually the sliding occurs in areas at the margins of the blade root and this sliding is defined as partial slip or microslip. The energy dissipated by the slip of surfaces and its amplitude depend mainly on the centrifugal force and the amplitude and phase of the oscillating forces.

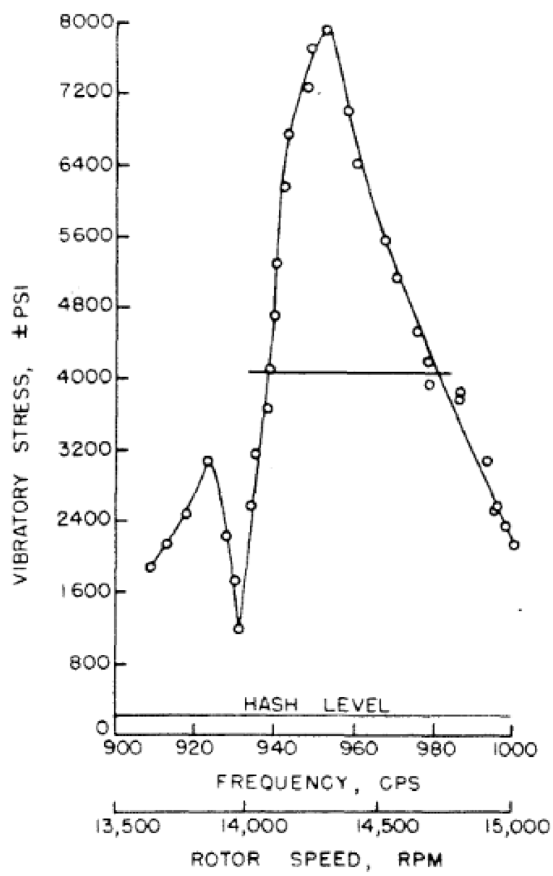

Figure 7: Blade vibration response in region of resonance [14]

During the years theoretical and experimental studies of the dumpling of the root section of the blade have been provided such as [23] that is one of the first published studies. After this publication a lot of research work were provided. In [14] the vibration produced by an axial flow compressor were studied in order to discover how is possible to minimize and in the report are discussed the factors affecting the vibration and the suppression of vibration. In [13] the operating temperature in a disc of a gas turbine engine are studied in order to discover the operating stress, rim cracking and how to provide the cooling. In

the turbine blades vibration are studied. In [8] a study focused on the vibration damper for axial flow compressor blading is proposed.
The first study focused on the friction damping correlated to the blade root joint was published my Goodman and Klumpp in the 1956 [6]. In this paper the friction in the area between the blade root and the disk is identified as a damping agent to reduce the turbine blade resonant stresses. Is presented a theory derived from the Coulomb friction focused on the energy dissipation in joints.

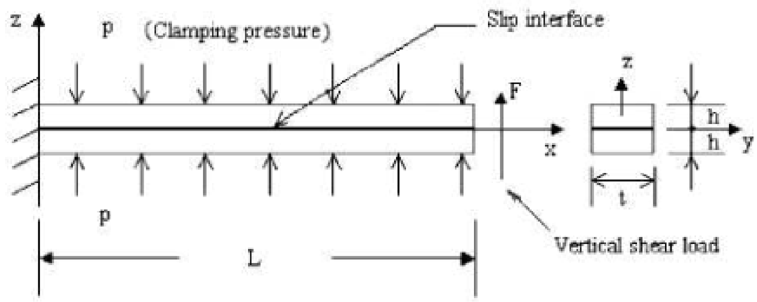

Figure 8: Joint geometry with loads applied [6]

The theory is developed and experimentally applied to a simple joint geometry in order to prove the numerical result obtained. The joint is summarized as a cantilever beam, figure 8, and the clamping pressure P is applied in both sides of the cantilever beam. The slip interface is located in the middle. Changing the clamping pressure P is possible to obtain a different clamping pressure in the middle section of the model and the theory developed in this paper demonstrate that the energy loss per cycle is a function of the normal pressure as is possible to see in the figure 9.

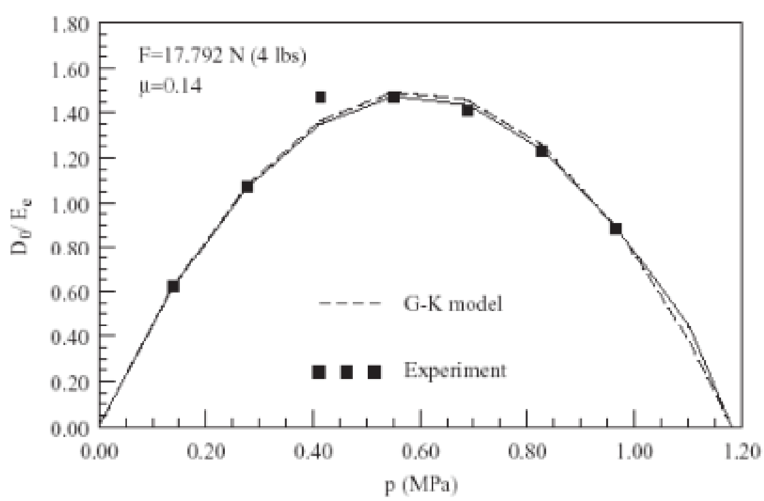

Figure 9: Variation of energy loss per cycle with joint normal pressure; comparison between theoretical and experimental results [6]

The energy loss per cycle function presents a maximum for a certain value of clamping pressure P, so is possible to obtain the optimal contact pressure. However the study explain that for the fir-tree or dovetail joints the values of slip damping are never achieved and with high centrifugal load force the optimal value of clamping pressure is obtained almost during the start of the engine.

Another study was conducted by Jones [10] and is a more realistic approach than [6] because it involves a real geometry. In this study a simple two mass analytical system of the blade is developed and is permitted the slip in the root blade-disk region. In the figure 10 the two masses and the slip region can be identified. The centrifugal load is applied to the blade using two spring and for the ring test a heavy fixation case is used. The centrifugal force applied to the blade is from 100 N to 200 N and the blade is excited by a transducer. This experiment shows that the apparent modal damping in a simple dovetail blade can be predicted on the basis of assumed gross slip. The investigation, however, is for a simple problem, but some interesting results were produced.

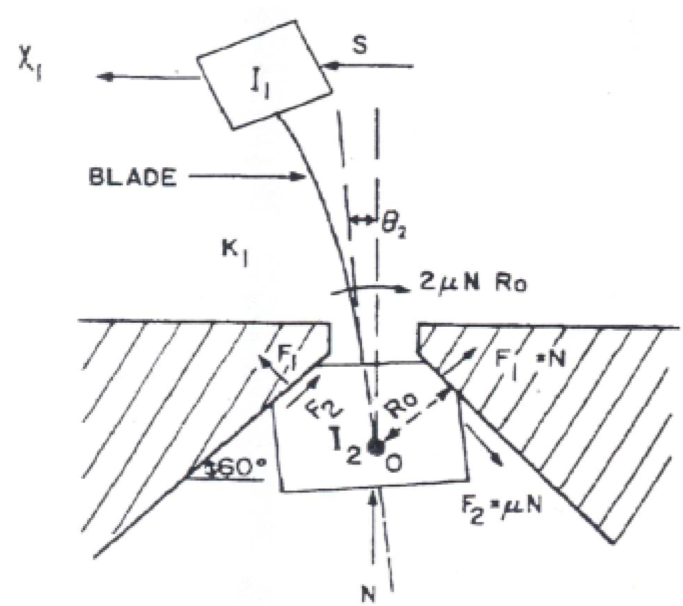

Figure 10: Dynamic system of two masses

In the NASA report [27] the aim was to investigate the materials for a gas turbine engine blade and discover their damping properties. A comparison of the experimental and numerical data is obtained and for the test a real root blade was used. The scale of the loads applied in the root of the blade were from 0.5 kN to 3 kN and the load is transmitted to the geometry using a roll bearing. As in the other articles a sinusoidal excitation is applied to the system and one of the focus was to obtain the maximum blade feedback in the resonance frequency.
Following the conclusion of this article and the figure 12 is possible to notice that the loss factor γ decrease exponentially rising the axial load. Another conclusion that is noticeable from this paper is that the damping properties are high under low axial loads as [6] also presented, so the damping properties are obtained for low engine speeds. Continuing with the conclusion of this paper is proved that the loss factor decrease at insignificant values for high axial loads, this condition means that the non-friction damping loss factor is adopted for high rotational speed of the gas turbine engine. Under these operating conditions the friction damping could be governed by microslip or local slip condition.

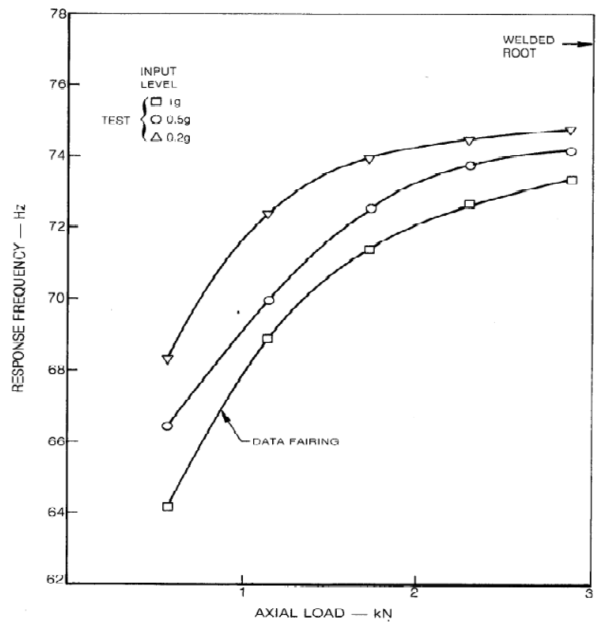

Figure 11: Variation of blade response frequency with root normal load for various excitations levels [27]

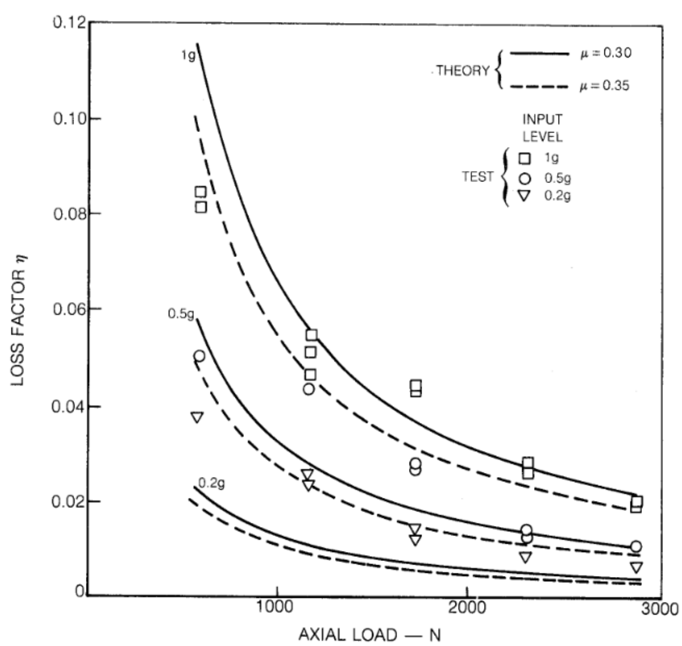

Figure 12: Variation of blade loss factor and axial load [27]

In [19] and [18] other studies focused in the damping characteristics in a gas turbine engine blade were performed. In the first work the bladed disk runs in a vacuum atmosphere in order to delete the aerodynamic damping that can be present if the atmosphere involved in the study presents a pressure. In the figure 13 is possible to see the shape of the disk and the shape of the blade in different sections.

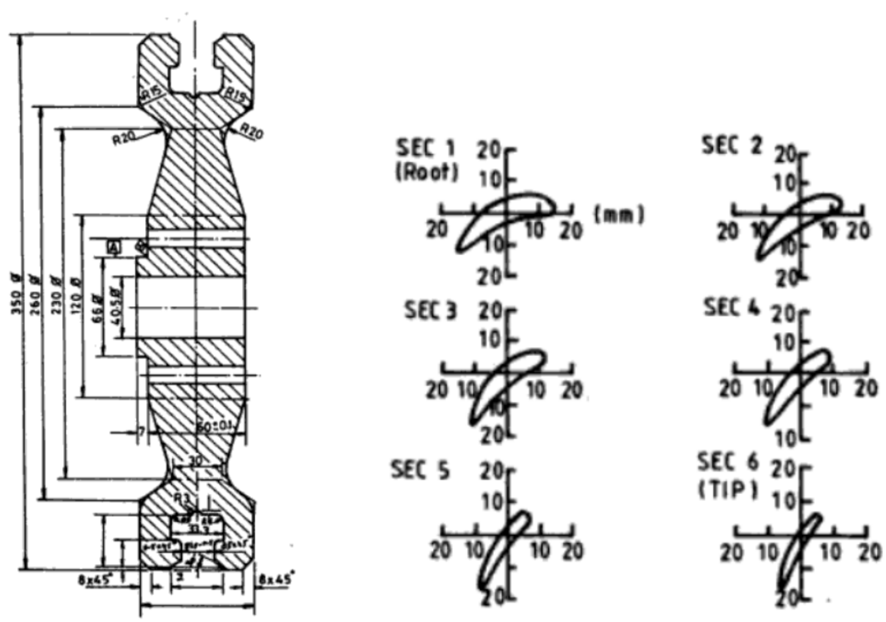

(a) *disk general view* (b) *shape of the blade*

Figure 13: details from [19]

The experiment set-up presents a bladed disk that runs at constant speed with electromagnetic excitation on it. In the first part of the experiment the damping is evaluated switching off the excitation and comparing the time of decay of the vibrations in the blades. Is possible to notice in the conclusion of this work that the modal response is similar in the first four modal nodes as illustrated in the figure 13 and the damping values decrease with the speed of rotation. As is already exposed in this work also [19] noticed that after $400rpm$ the variation of modal damping is negligible indicating a predominantly root damping effect. For higher rotational speed the damping effects of the root tends to decade and the modal damping values increase with the strain amplitude as is possible to notice in the figure 14 where is presented the damping ratio correlated to the strain amplitude for different engine speed.

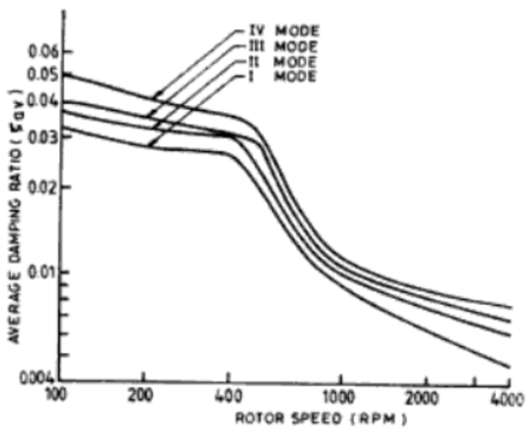

(a) *damping ratio and rotor speed*

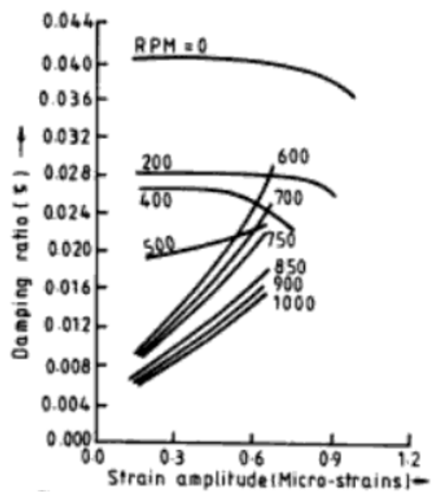

(b) *damping ration and strain for the first mode*

Figure 14: Details from [19]

Experiments on real elements were performed in [11] where kielb and Abhary tested a bladed turbine disk in different conditions. The experimentation process is divided in two phases. In the first part of the work the elements ran under thermal, pressure and speed loads in order to obtain some useful data. In the second part of the experiment the elements ran in a vacuum chamber with an artificial excitation. The conclusion indicates that the aerodynamic forces acting on the system have a relevant effect especially in damping. As is possible to notice in the 15 the friction damping coefficient decrease increasing the rotational speed of the engine as is demonstrated in other papers.

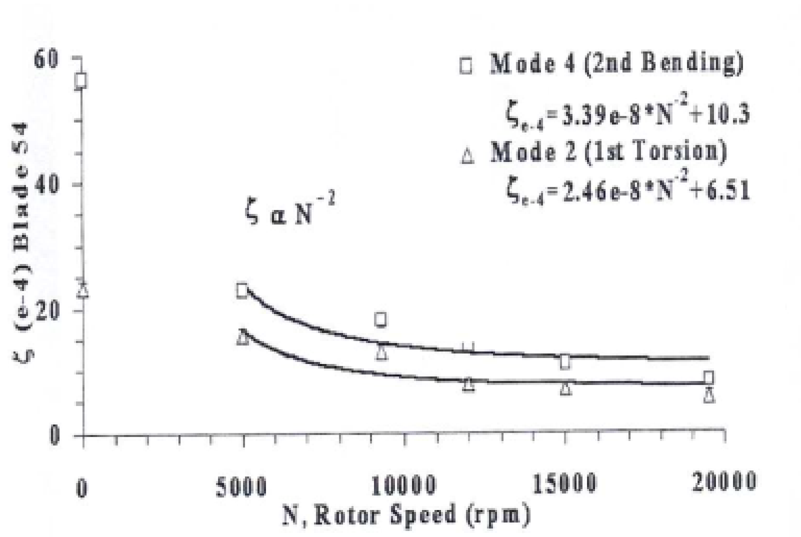

Figure 15: structural damping and engine speed

In [5] a multi harmonic balance method is proposed in order to investigate the the forced response of bladed disks and the non-linearity friction activities in blade roots. A bladed disk was tested in a vacuum chamber and the excitation was transferred by a piezoelectric actuator. A DLFT method (Dynamic Lagrangian Frequency Time) is studied in order to compute the steady state response of the structure where friction and contact takes place. In the figure 16 is presented the calculating process of the method proposed using node-to-node elements.

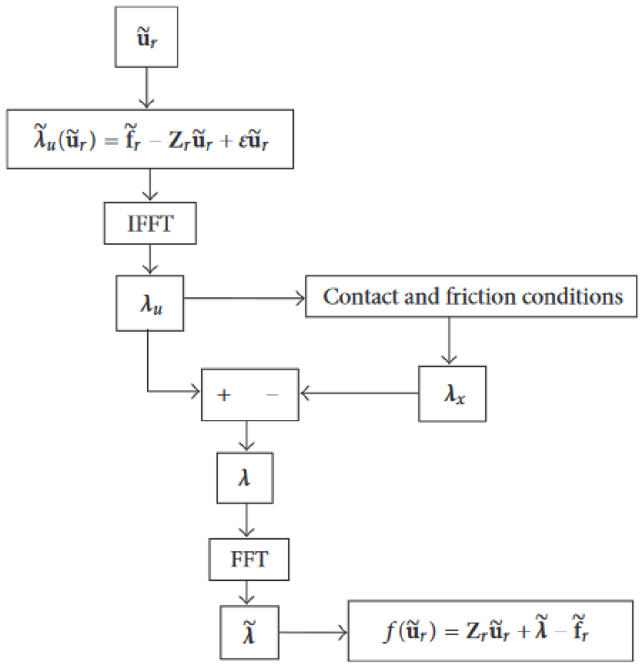

Figure 16: DLFT method procedure

An experimental test is performed in order to verify the numerical results obtained. During the test only friction were considered and the blade has a dovetail type connection with the disk. The aerodynamic effects were decreased thanks to the vacuum atmosphere and real gas turbine engine blades were used as is showed in the figure 17.
The set-up of the experiment presents a disk with two pairs of blades placed in opposite pair in order to achieve the balancing condition while the disk rotates thanks to an electric motor and a two bearing shaft. Five rotational speed were studied from 1000 rpm to 5000 rpm and different level of excitation were provided. The evidence of non linearity is demonstrated and also the resonance on the second mode. The behaviour of the blade could be assumed as linear for low-frequency, but non-linear near the resonance frequency attributed to the blade root friction. A finite element model is produced and numerical and experimental results compared applying the DELFT method described before. The results of the numerical method are very similar to the experiment, but some discrepancy appeared correlated to the assumptions and the accuracy during the calculations. In the figure 18 some results are compared.
In [20] different publications are compared and the state of art of the different methods to analyse a mechanical system under dry friction contact are explained.

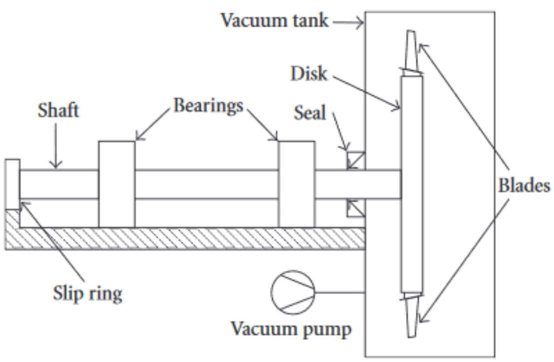

(a) *schematic view of the experiment*

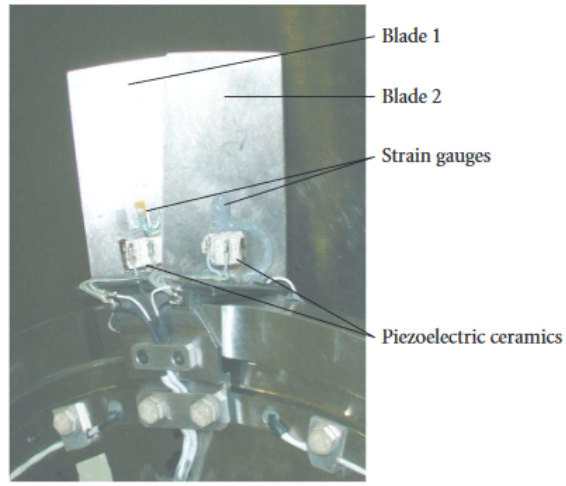

(b) *blade involved in the experiment*

Figure 17: details of the experiment [5]

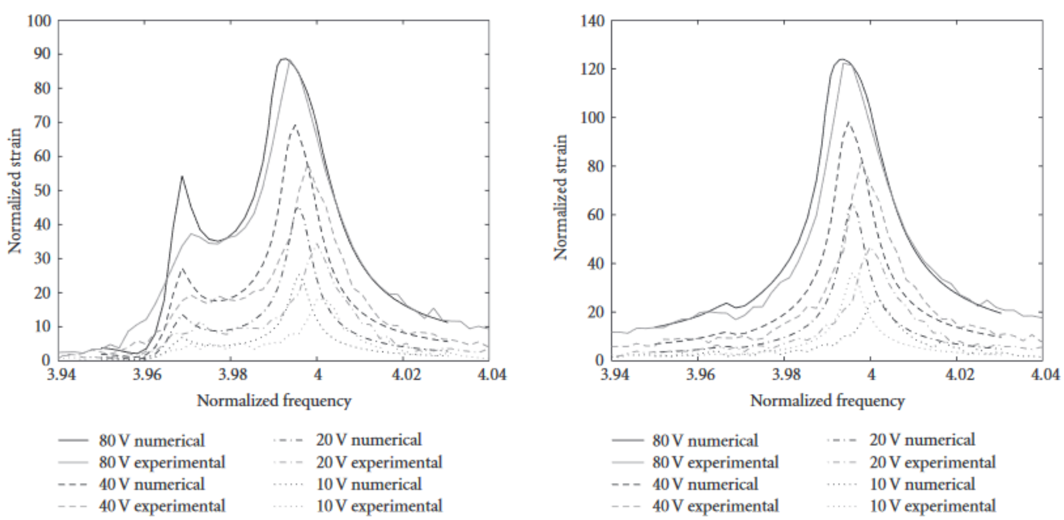

Figure 18: numerical and experimental results at $3000rpm$

2 Dummy blade

2.1 Introduction

Modelling The model of the blade is firstly designed using Simens NX following the dimensions of the real model in order to produce the effective accuracy. Essentially the preliminary part is divided in two main section:

1. 3D modelling of the experiment geometry using Simens NX software
2. converting the 3D model into a parasolid file.

Parasolid is geometric modelling kernel compatible with the NX 3D elements and one of its particularities is that it uses boolean modelling operators. In the figure 19 is possible to notice that the blade is divided in different elements.

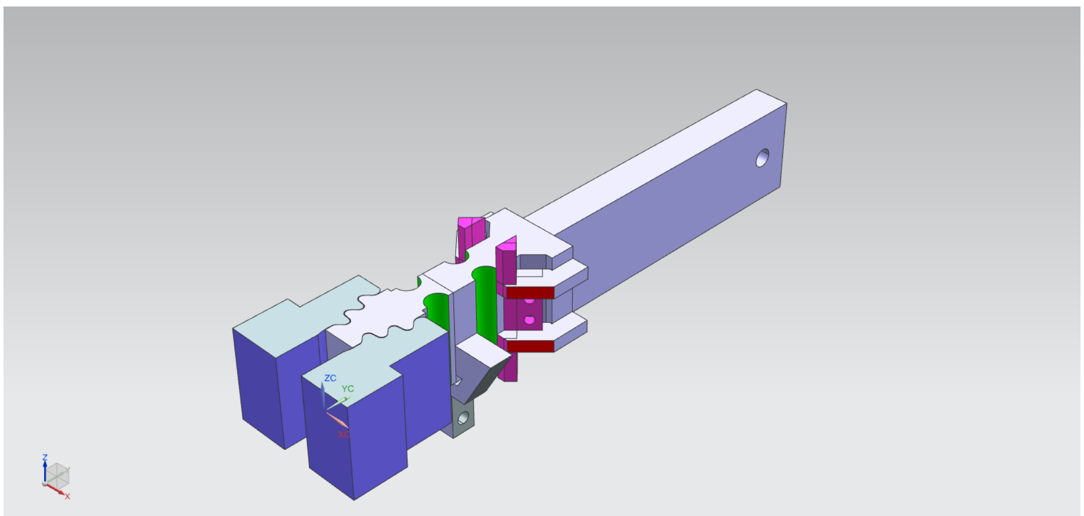

Figure 19: View of the parasolid blade assembly

The system, as is possible to see in the figure 19, is divided in several parts in order to consider it separately during the mesh and defining loads procedure.
The model is a replication of the ring test set-up of the experiment produced in [3]. In this experiment relative displacements and forces in the contact surfaces are measured. Is is illustrated in the figure 20 the position of the replaceable contact pads that are on contact with the blade and the ground platform. The centrifugal force is artificially obtained through an adjustable clamping force. Dumper contact forces on the ground platform are measured as the relative displacement between the contact surfaces.

Related academic papers The blade used in the test is a fir-tree root and the conditions of the test reflect the real load conditions that a gas turbine engine blade has to endure and different centrifugal forces are tested. The exciting force is transmitted to the blade in the top section of the blade and different values are performed. The acceleration at the tip of the blade is plotted as a function of the excitation frequency.
In this section of the thesis similar numerical-based results are obtained. Numerical and experimental data are compared.

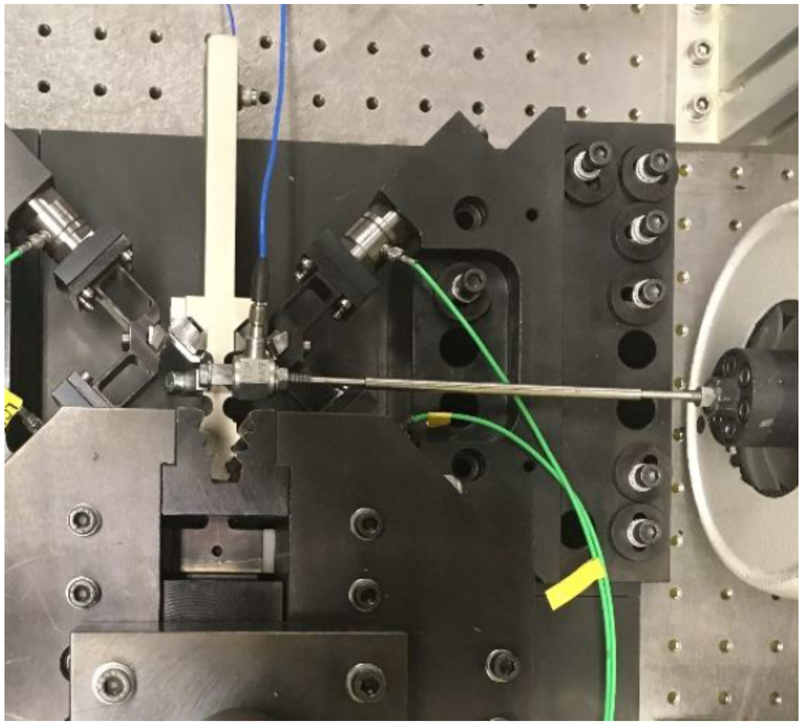

Figure 20: Ring test set-up in [3]

As already proved in others research works the non-linearity behaviour is evident because of the friction behaviour in the root section of the blade. Performing the ring test is possible to analyse the damping abilities and the hysteresis loop. With the hysteresis plot is possible to analyse the gross-slip and micro-slip and evaluate its performance. In this study numerical and experimental results about the hysteresis loop are compared for different contact forces.

In [29] the behaviour of the under-platform dumper is investigated focusing on the contact characteristics and damping abilities. The stiffness of the system depends from K_c and μ and considering also the damping is possible to obtain the contact characteristics. This papers investigate the macro behaviour of the dumper related to the micro/local behaviour of the contact region. The test was performed using a real turbine blade made single crystal nickel based alloy and the centrifugal force is transmitted to the blade using two cylindrical elements. The analysis is divided in two parts. The firs part is focused on the standard FRF for different excitation force values for each static force level of the dumpers. The blade is excited trough an electromagnetic shaker. The second part of the study analyse the displacement and the relative velocity between the blade and the damper. The system is tested with both static and excitation force at the same amplitude level of the first part of the study. The equivalent characteristics of damping C_{eq} and equivalent tangential stiffness K_{eq} are calculated.

A numerical system is proposed in order to compare the equivalent contact damping and stiffness with a single degree of freedom.

The blade tip acceleration is compared to the equivalent damping C_{eq}.

The behaviour of the equivalent stiffness and damping is demonstrated numerically in a previous section.

2.1.1 Theory of the model

Cylindrical Hertzian Contact The cylindrical Hertzian Contact problem is vastly described in the literature ([31], [21], [25]) and Poritsky in the 1950 [17] wrote a famous paper and he described how the Hertzian contact is used in the gears and in the train wheels. The Hertzian contact in those years was vastly investigated in order to increase the efficiency of the railway system. In [17] the share traction distribution is:

$$q(x) = \frac{2Q}{\pi b}\sqrt{1-(\frac{x}{b})^2} \tag{3}$$

where b is the with of the half area of the bodies in contact and Q is the tangential load divided the length. Is possible to calculate the displacements on the area:

$$\mathrm{u(x)} = \frac{2\mathrm{Q}}{\pi \mathrm{E}^*}\left(\frac{\mathrm{x}}{\mathrm{b}}\right)^2 + \mathrm{C}_1 \quad \text{if } |\mathrm{x}| \leq \mathrm{b} \tag{4}$$

$$\mathrm{u(x)} = \frac{2\mathrm{Q}}{\pi \mathrm{E}^9}\left(\ln\left(\left|\frac{\mathrm{x}}{\mathrm{b}}\right| + \sqrt{\left(\frac{\mathrm{x}}{\mathrm{b}}\right)^2 - 1}\right) + \frac{1}{2}\left(\left(\frac{\mathrm{x}}{\mathrm{b}}\right) + \sqrt{\left(\frac{\mathrm{x}}{\mathrm{b}}\right)^2 - 1}\right)^{-2}\right) + \mathrm{C}_2 \quad \text{if } |\mathrm{x}| \geq \mathrm{b} \tag{5}$$

The total slip of the bodies can be defined multiply the displacement produced. So the displacement is:

$$s(x) = 2q(x) \tag{6}$$

And the constant $C1$ and $C2$ are not considered because in the stick region the displacement produced is zero. Is possible to notice that the displacement in the contact surfaces are maximum in the extremes $x/b = [-1;1]$ and is zero in $x/b = 0$. In the Poritsky paper the evaluation of the dissipated energy E is provided as well as the damage parameter D in the event of sliding.

$$D_{lim} = \frac{\mu^2 Pb}{\pi R}\left(\frac{x}{b}\right)^2\sqrt{1-\left(\frac{x}{b}\right)^2} \tag{7}$$

The equation of the dissipated energy is manipulated and is obtained in the following form:

$$\mathrm{E_{Lim}} = \left(\frac{2}{\pi}\right)^2 \frac{(\mu \mathrm{P})^2}{\mathrm{E}^*}\left[\frac{1}{8}\left(\mathrm{t}\sqrt{1-\mathrm{t}^2}\left(2\mathrm{t}^2-1\right) + \mathrm{a}\sin(\mathrm{t})\right)\right]\Bigg|_{-1}^{1} = \left(\frac{2}{\pi}\right)^2 \frac{(\mu \mathrm{P})^2}{\mathrm{E}^*}\cdot\frac{\pi}{8} \tag{8}$$

As is suggested from [2] is possible to use the dimensionless form of the energy and for the entire cycle of full load the energy dissipated is:

$$\frac{E_{\mathrm{lim}}}{\left(\frac{2}{\pi}\right)^2 \frac{(\mu P)^2}{E^*}} = \frac{\pi}{2} \tag{9}$$

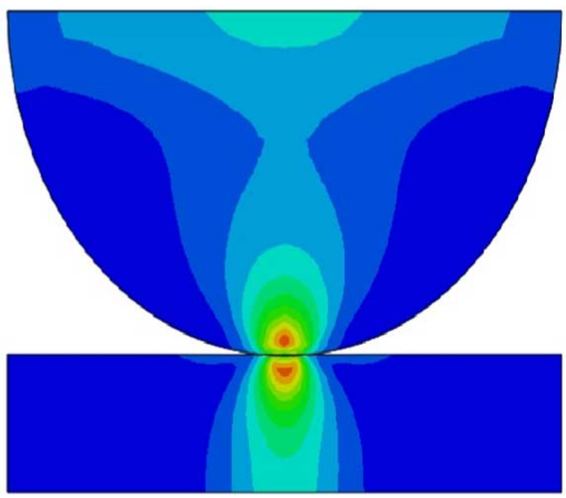

Figure 21: Hertz contact simulation [30]

FEM Analysis The analytical formulation of the method described in [24] is integrated with a Finite Element Model (FEM). The Finite Element (FE) technique is vastly described by different academic papers. The system is divided into a large number of smaller systems or parts (the finite elements) and a mesh is built. This part is the domain of the numerical calculation and using different calculus methods is possible to obtain a solution minimizing the errors. The ambient of the solution is called Finite Element Analysis (FEA) and its goal is to solve the analytical systems produce by the FE calculation. The main advantages of a FE method can be summarise in:

1. analysis of complex geometries
2. analysis of the system with various constrains
3. analysis of the system with various load applied

On the other hand the FE analysis presents some limitations that can be resolved the most of time with a precise analysis of the problem and setting of the solver. The main disadvantages of a FE method can be summarise in:

1. non-solving possibility of the system
2. errors in the mesh creation
3. human decisions related to the solving procedure
4. amount of memory required for the calculation

In this thesis the FE Analysis is performed using Ansys Mechanical 18.2. In a first approximation the FEM is focused to solve the following equation for each node:

$$[\mathrm{K}]\{\mathrm{D}\} = \{\mathrm{R}\} \rightarrow \{\mathrm{D}\} = [\mathrm{K}]^{-1}\{\mathrm{R}\} \tag{10}$$

where $[K]$ is the global stiffness matrix, $\{\mathrm{D}\}$ is the vector of total number of nodes taking in account the degree of freedom, $\{\mathrm{R}\}$ is the load vector of each node.

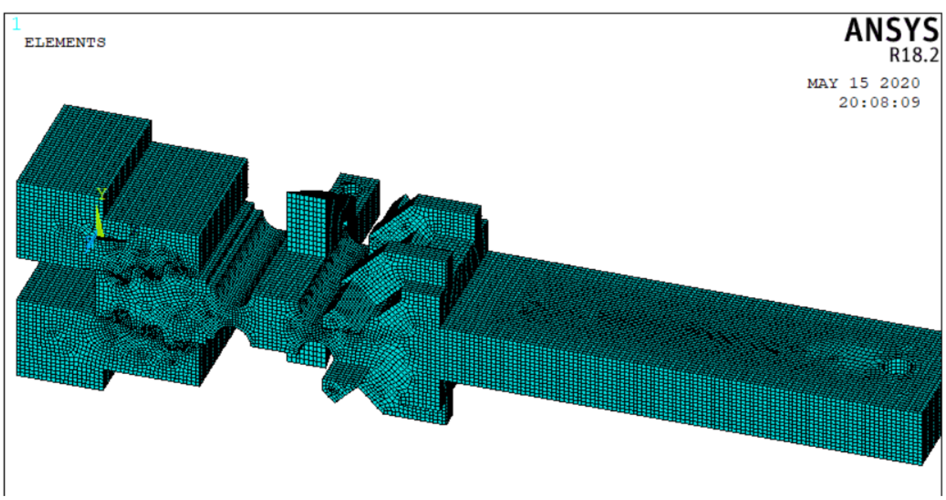

Figure 22: FE mesh of the dummy blade under study

Theory of contact The contact iterations between two bodies are vastly described in the literature and theirs study is essential to understand the dynamic behaviour of a system. The forces produced by the contact iteration of two bodies produce a non-linear behaviour and dynamic responses such gross-slip or micro-slip. In the figure 23 is possible to notice slip and stick areas under fretting contact. In this thesis the contact between the root of

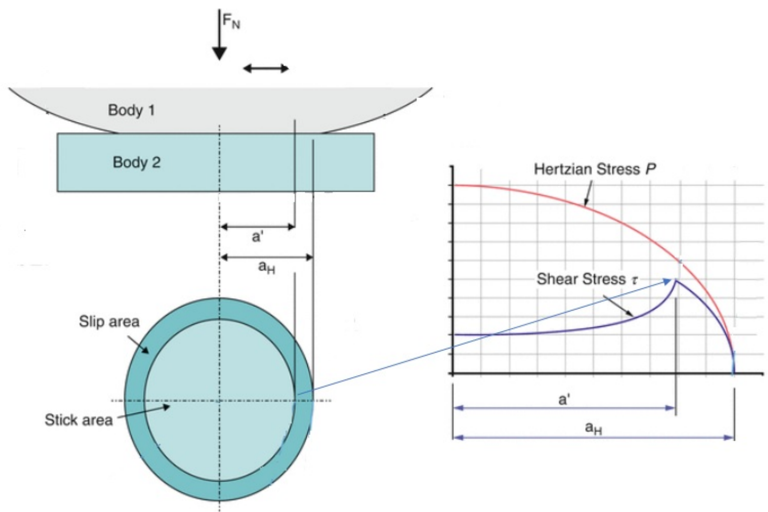

Figure 23: Stick and Slip region

the blade and the disk is studied in two different models. The first model is visible in the figure 22 and the second model respect a real model of a gas turbine engine bladed disk. The following explanation is mostly based on the theory described in [2], [7] and [24]. The hysteresis cycle, explained and showed in the figure 6, is at the basic of the theory because it correlates the displacement δ between the two bodies and the tangential contact forces. In the figure 24 are illustrated the main parameters of two bodies in contact and O represent the stick central region. After the application of the tangential force Q the two points $A1$ and $A2$, coincident if $Q = 0$, separate and two rigid displacements are produced. The rigid displacements are δ_{x1} and δ_{x2} and the elastic displacements u_{x1} and u_{x2} are correlated to the measurements $T1$ and $T2$ respectively. The absolute displacement in the x direction is S_x and the literature explain that is possible to achieve the absolute displacement.

$$S_x = S_{x1} - S_{x2} \tag{11}$$

$$S_{x1} = (u_{x1} - \delta_{x1}) \tag{12}$$

than is possible to write the final expression

$$S_x = (u_{x1} - u_{x2}) - (\delta_{x1} - \delta_{x2}) \tag{13}$$

In the slip region $S_x > 0$, but in the stick region the absolute displacement is zero. Than is possible to evaluate the displacement:

$$(u_{x1} - u_{x2}) - (\delta_{x1} - \delta_{x2}) = \delta_x \tag{14}$$

In our case of study, the bladed disk, the characteristic dimension of the problem is big enough to let us to assume δ as the displacement of the contact. In the root of a blade

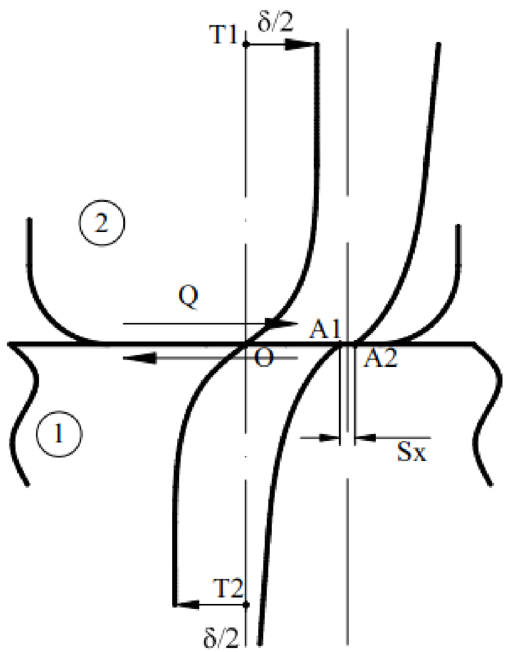

Figure 24: Relative motion between two bodies [2]

the contact pressure, thanks to the high centrifugal force and the low area involved, is generally significant. In this region if the displacement involved are small the hysteresis cycle can evidence two kind of displacement:

1. microslip
2. gross-slip or macroslip

The gross-slip appear if the tangential force τ exceed the value of the limit of static friction μN. In this condition full surface slide and the hysteresis cycle have the shape represented in the figure 25. In the gross-slip hysteresis cycle is possible to notice that the displacement increase in condition of constant load. The microslip presents a non-linear behaviour

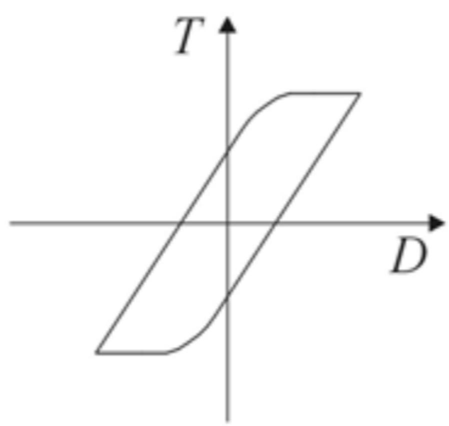

Figure 25: Gross-slip hysteresis cycle shape

and this condition occurs when the tangential load can not overcome the static friction coefficient. In the zone of contact two conditions appears simultaneously:

1. in the stick region the displacement appears rigid and there is no movement between the bodies
2. in the slip region there is sliding between the two bodies

The hysteresis loop is represent in the figure 26 The harmonic balance method is used

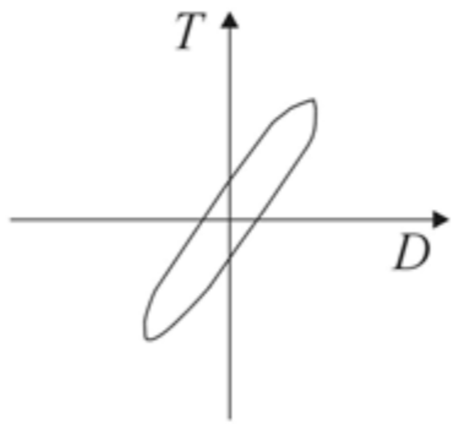

Figure 26: Microslip hysteresis cycle shape

to solve the systems that present simultaneity static dynamic response. Is described and investigated in different papers such as [16] or [22]. In this thesis the experimental approach is used and a numerical way to calculate the hysteresis cycle, based on the mathematical approach in [2], is performed.

Contact model In order to evaluate the hysteresis cycle in the contact region of our system is needed to impose some assumptions . Those assumptions allow us to solve the analytical calculation ([7]) and obtain a solution that can be used to implement the numerical model for the study. The hypothesis adopted are the following:

1. the bodies are isotropic
2. the material in the bodies is perfectly elastic and the elastic limit is not reached
3. the surfaces under contact are planar and their roughness is not considered. This hypothesis allow the imply that the contact is continuous.
4. the contact region of the blade root is transformed into a correspondent region suitable for the calculation represented in the figure 27. The half plane idealization is used ([2]) because the ratio between the length of the flat area $[-c; c]/2$ and the radius R is small. If the ratio becomes bigger the assumption is not valid and more parameters of the geometry has to be considered

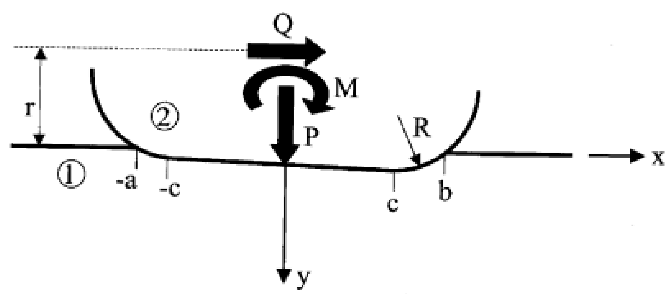

Figure 27: Contact scheme

5. the friction coefficient μ is defined for every region of contact behaviour. As represented in the figure 23 the area of contact has two regions and every region has its Amonton's law of friction:
   (a) in the slip region:
   $$|q(x, y)| = \mu|p(x, y)| \tag{15}$$
   (b) in the stick region:
   $$|q(x, y)| \leq \mu|p(x, y)| \tag{16}$$
6. the variation of the dynamic loads in the region of contact follow a sinusoidal law. In this case is assumed that the normal load on the contact surface is constant, so the vibrational loads are not taking in account.
7. the share and normal loads are evaluated using the theory of 2D contact problem.

Normal pressure and Share traction The contact problem for a flat and round edge surface, as in the figure 27, is investigated form different authors as [4]. Here the theory is summarized. The function that describe the shape of the contact problem is:

$$\mathrm{h(x)} = \begin{cases} \frac{(\mathrm{x+a})^2}{2\mathrm{R}} & \text{if} \quad -\mathrm{b} \leq \mathrm{x} \leq -\mathrm{a} \\ 0 & \text{if} \quad -\mathrm{a} \leq \mathrm{x} \leq \mathrm{a} \\ \frac{(\mathrm{x-a})^2}{2\mathrm{R}} & \text{if} \quad \mathrm{a} \leq \mathrm{x} \leq \mathrm{b} \end{cases} \tag{17}$$

The solution of this equation is only for elastic bodies, that is an assumption, and is not taken in account that the coupling and the pressure distribution can be affected form the share traction. In order to evaluate the pressure distribution some parameters need to be calculated such as:

1. composite stiffness E^* because the two bodies are in contact:

$$\frac{1}{\mathrm{E}^*}=\frac{1}{\mathrm{E}_1}\left(1-v_1^2\right)+\frac{1}{\mathrm{E}_2}\left(1-v_2^2\right) \tag{18}$$

2. this implicit equation is needed to evaluate ϕ:

$$\frac{4\mathrm{PR}}{\mathrm{a}^2\mathrm{E}^*}=\frac{\pi-2\varphi_0}{2\sin^2\varphi_0}-\cot\left(\varphi_0\right)=\frac{\pi-2\varphi_0-2\sin\varphi_0\cos\varphi_0}{2\sin^2\varphi_0}=\frac{\pi-2\varphi_0-\sin 2\varphi_0}{2\sin^2\varphi_0} \tag{19}$$

   The parameter

$$\mathrm{f}=\frac{4\mathrm{PR}}{\mathrm{a}^2\mathrm{E}^*} \tag{20}$$

   represents the shape of the surface. More f parameter is high it means that the surface is curved and its lead infinite if the surface can be represented as cylindrical.

Than is possible to evaluate the pressure distribution using the following formula:

$$\frac{\mathrm{bp}(\varphi)}{\mathrm{P}}=\frac{2/\pi}{\pi-2\varphi_0-\sin 2\varphi_0}\left\{(\pi-2\varphi_0)\cos(\varphi)+\ln\left[\begin{array}{c}\left|\frac{\sin(\varphi+\varphi_0)}{\sin(\varphi-\varphi_0)}\right|^{\sin\varphi} \\ \cdot\tan\frac{\varphi+\varphi_0}{2}\tan\frac{\varphi-\varphi_0}{2}\Big|^{\sin\varphi_0}\end{array}\right]\right\} \tag{21}$$

In this thesis an Ansys Mechanical code, which reflect the theory of contact and the evaluation methods mentioned, is used. In the figure 28 the formula 21 is inserted in the code. It is noticeable that the pressure distribution function reaches a maximum in the

```
*DIM,nload%j%,ARRAY,nb+1,2,1, , ,
*do,x_i,1,nb+1
xx=(-b+2*b*(x_i-1)/nb)
f_i=asin((-b+2*b*(x_i-1)/nb)/b)

F=2/pi/(pi-2*fo-sin(2*fo))*((pi-2*fo)*cos(f_i)+log(abs(sin(f_i+fo)/sin(f_i-fo))**sin(f_i)*abs(tan((f_i+fo)/2)*tan((f_i-fo)/2))**sin(fo)))

nload%j%(x_i,1)=(-b+2*b*(x_i-1)/nb)
nload%j%(x_i,2)=F*P/b !*(2*b/nb)

*if,xx,eq,0,then
xx=1e-30
*endif

XTIME(x_i)=xx
XFUNC(x_i)=F*P/b*log(abs((L/2+sqrt(xx**2+(L/2)**2))/xx))

*enddo
```

Figure 28: Normal pressure distribution equation code

extremis of the contact surface and can be represented as the Hertzian case in the center of the contact region where $x = 0$.
The share traction is evaluated in condition of constant normal load and the tangential load increased because the variation caused from the vibration load is not taken into account. The tangential traction [4] is evaluated:

$$\mathrm{q(x)}=\mu\mathrm{p(x)}-\mathrm{q}^*\mathrm{(x)} \tag{22}$$

and taking into account the relation $\sin\varphi = \frac{x}{b}$ and $\sin(\vartheta_0) = \frac{\mathrm{a}}{\mathrm{c}}$ is possible to evaluate the following formula:

$$\frac{\mathrm{c}q^*(\vartheta)}{\mu\mathrm{P} - \mathrm{Q}} = -\frac{2/\pi}{\pi - 2\vartheta_0 - \sin 2\vartheta_0} \left\{ (\pi - 2\vartheta_0)\cos\vartheta + \ln\left[\left|\frac{\sin(\vartheta+\vartheta_0)}{\sin(\vartheta-\vartheta_0)}\right|^{\sin\vartheta} \cdot \left|\tan\frac{\vartheta+\vartheta_0}{2}\tan\frac{\vartheta-\vartheta_0}{2}\right|^{\sin\vartheta_0}\right]\right\} \quad (23)$$

which is represented in the Ansys Mechanical code as illustrated in the figure 29. In possible

```
*do,x_i,1,nb+1
xx=(-b+2*b*(x_i-1)/nb)

f_i=asin((-b+2*b*(x_i-1)/nb)/b)

F=2/pi/(pi-2*fo-sin(2*fo))*((pi-2*fo)*cos(f_i)+log(abs(sin(f_i+fo)/sin(f_i-fo))**sin(f_i)*abs(tan((f_i+fo)/2)*tan((f_i-fo)/2))**sin(fo)))

tload%j%(x_i,1,q_i)=(-b+2*b*(x_i-1)/nb)
tload%j%(x_i,2,q_i)=FC*F*P/b

*if,xx,eq,0,then
xx=1e-30
*endif

XTIME(x_i)=xx
XFUNC(x_i)=-(FC*F*P/b*log(abs(xx/b)))
! XFUNC(x_i)=FC*F*P/b*((1-nu1)*log(abs((L/2+sqrt(xx**2+(L/2)**2))/xx))+nu1*(L/2)/sqrt(xx**2+(L/2)**2))

*enddo
```

Figure 29: Share distribution equation code

to obtain an analogue relation, as showed in the equation 19, for the share traction and then the following relation is evaluated:

$$\frac{q(x)b}{P} = \frac{\mu p(x)b}{P} - \frac{q^*(x)b}{P} \quad (24)$$

In the figure 30 is possible to notice how the pressure distribution is distributed in the surface of contact and its variation due different normal and tangential force ratios. The

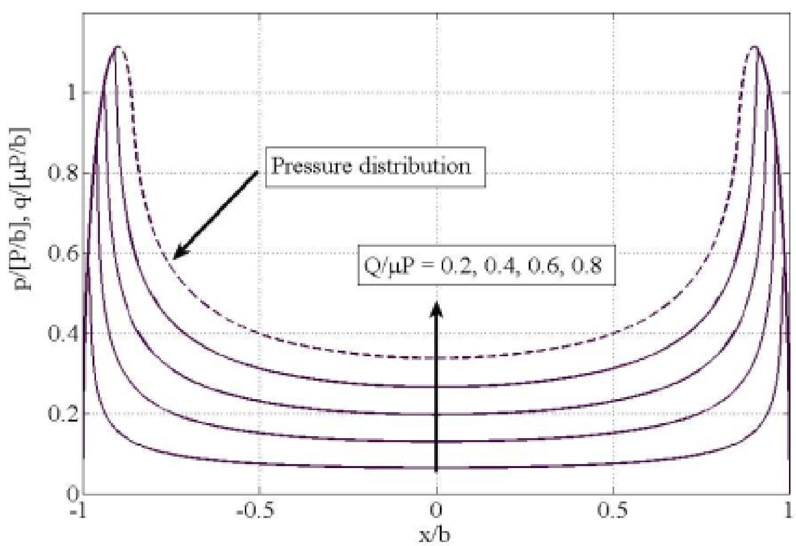

Figure 30: Pressure distribution [2]

pressure distribution increase if the force ratio increase and in the extremis of the graph the pressure reach a maximum. This point represented in the figure 31 represents the stick zone limit for a perfectly planar contact surface without penetration.

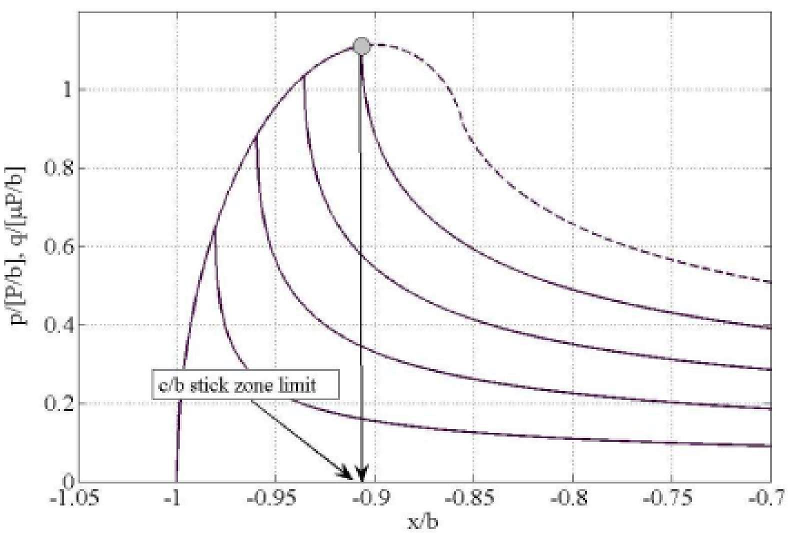

Figure 31: Pressure distribution focus [2]

Relative displacements and Energy dissipated The surface in relative contact can move reciprocally and as already explained the problem is reduced to a two dimension problem. The stick zone in the contact surface is where the displacement is zero, so if the strain of the surfaces in known is possible to integrate the relative displacements from the stick zone. The relative displacements are essentially and thanks to them is possible to calculate the dissipated energy in the microslip region. As demonstrated in [9] the displacement can be calculate once the normal pressure and the share traction are evaluated because those values must be inserted in the integral calculation.

$$\mathrm{u_x} = -\frac{(1-2v)(1+v)}{2\mathrm{E}}\left\{\int_{-\mathrm{b}}^{\mathrm{x}} \mathrm{p(s)ds} - \int_{\mathrm{x}}^{\mathrm{a}} \mathrm{p(s)ds} -\right\} - \frac{2\left(1-v^2\right)}{\pi \mathrm{E}}\int_{-\mathrm{b}}^{\mathrm{a}} \mathrm{q(s)} \ln|\mathrm{x}-\mathrm{s}|\mathrm{ds} + \mathrm{C_1} \tag{25}$$

$$\mathrm{u_2} = -\frac{2\left(1-v^2\right)}{\pi \mathrm{E}}\int_{-\mathrm{b}}^{\mathrm{a}} \mathrm{p(s)} \ln|\mathrm{x}-\mathrm{s}|\mathrm{ds} + \frac{(1-2v)(1+v)}{2\mathrm{E}}\left\{\int_{-\mathrm{b}}^{\mathrm{x}} \mathrm{q(s)ds} - \int_{\mathrm{x}}^{\mathrm{a}} \mathrm{q(s)ds} -\right\} + \mathrm{C_2} \tag{26}$$

After some manipulations of the displacement equations is possible to evaluate the displacement relative to a common coordinate system and the slip S can be calculated:

$$\mathrm{S} = \mathrm{u_{x1}} + \mathrm{u_{x2}} \tag{27}$$

In case of contact between two elements with the same material properties is possible to transform the general equation:

$$\begin{aligned}\mathrm{S} = &\left(-\frac{(1-2v_1)(1+v_1)}{2\mathrm{E_1}} + \frac{(1-2v_2)(1+v_2)}{2\mathrm{E_2}}\right)\\ &\left\{\int_{-\mathrm{b}}^{\mathrm{x}} \mathrm{p(s)ds} - \int_{\mathrm{x}}^{\mathrm{a}} \mathrm{p(s)ds}\right\} - \left(\frac{2\left(1-v_1^2\right)}{\pi \mathrm{E_1}} + \frac{2\left(1-v_2^2\right)}{\pi \mathrm{E_2}}\right)\\ &\int_{-\mathrm{b}}^{\mathrm{a}} \mathrm{q(s)} \ln|\mathrm{x}-\mathrm{s}|\mathrm{ds} + \mathrm{C_1}\end{aligned} \tag{28}$$

in a more simplified equation:

$$\mathrm{S(x)} = -2\frac{2\left(1-\mathrm{v}^2\right)}{\pi \mathrm{E}}\int_{-\mathrm{b}}^{a} \mathrm{q(s)} \ln|\mathrm{x}-\mathrm{s}|\mathrm{ds} + \mathrm{C_1} \tag{29}$$

Where the constant C_1 is equal zero if the stick zone is assumed as rigid. The energy dissipated by the microslip can be obtained late all the parameters described above are evaluated simply integrate the work produced by the displacement in the slip area.

$$\mathrm{E} = \int_{\mathrm{A_{SLIP}}} \mathrm{S_x(x)} \cdot \mathrm{q_x(x)dx} \tag{30}$$

Hysteresis cycle Considering all the hypothesis and simplifications involved in our model is possible to take in account separately the pressure distribution and the share distribution. Starting from the Cerruti equations described in [2] is possible to only consider the displacement u_x results from the share traction. The hypothesis of the model allow us to separate the explanations and consider only the x axis displacement, that is useful for our calculation model because remembering the figure 27 the x axis is the direction where the share traction is applied. The reference system is presented in the figure 32 and according to the figure is possible to define reference position R:

$$R^2 = (x - r)^2 + (y - s)^2 + z^2 \tag{31}$$

and the displacement u_x:

$$\mathrm{u_x} = \frac{(1+v)}{\pi \mathrm{E}} \int_{-\mathrm{b}}^{\mathrm{b}} \mathrm{q_x(r)} \int_{-\mathrm{L}/2}^{\mathrm{L}/2} \left[\frac{(1-v)}{\sqrt{\mathrm{r}^2+\mathrm{s}^2}} + \frac{\mathrm{vr}^2}{(\mathrm{r}^2+\mathrm{s}^2)^{3/2}} \right] \mathrm{dsdr} \tag{32}$$

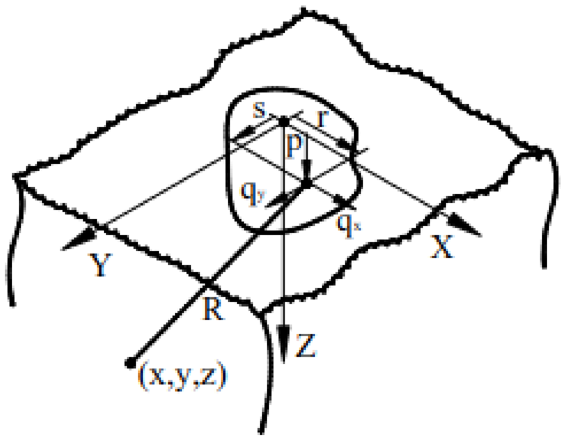

Figure 32: Reference system [2]

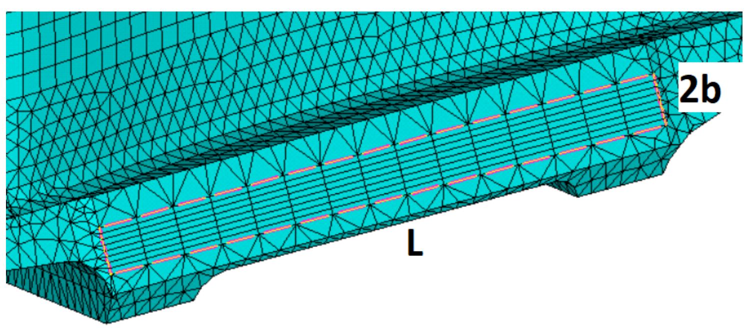

Figure 33: Dimension contact surface

Assuming that the L parameter is higher than $2b$, as is possible to see in the figure 33, the only unknown variable is the x. So after some manipulation is possible to calculate the total tangential deformation δ_x of the bodies in contact. This equation is requested once drawing the hysteresis cycle that is showed in the figure 34.

$$\delta_x = -2 \cdot \left[\frac{2 \cdot (1 - v^2)}{\pi E} \int_{-b}^{b} q_x(r) \lg\left(\frac{r}{b}\right) dr - \frac{2 \cdot (1-v^2)}{\pi E} \cdot \frac{Q}{L} \cdot \left(\lg\left(\frac{L}{b}\right) + \frac{v}{1-v} \right) \right] \tag{33}$$

The complex stiffness can be summarize with the following equation:

$$\mathrm{K_{Re}} + \mathrm{jK_{im}} = \frac{\mathrm{T_{Re}} + \mathrm{jT_{Im}}}{\mathrm{U}} = \frac{1}{\mathrm{U}} \frac{1}{\pi} \int_0^{2\pi} \mathrm{T}(\vartheta) \cdot \mathrm{e}^{-\mathrm{j}\vartheta} \mathrm{d}\vartheta \tag{34}$$

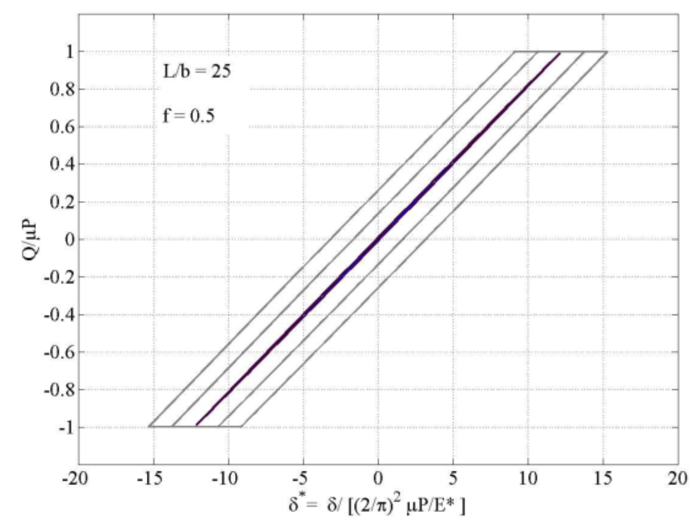

Figure 34: Hysteresis cycle [2]

Once the contact model is explained for a simple model, as showed in the figure 32, is possible to illustrate the general procedure used for a real system. The system under study in the bladed disk focused on its contact iteration between the root of the blade and the disk. The contact surface between the root of the blade and the disk is affected by a non-linear behaviour. Due the non-linear behaviour of the dynamic system and the characteristics of the rigidity the command EQSLV,SPARSE is added to the Ansys script in order to increase its solution ability.

```
/solu
EQSLV,SPARSE  !!!added for the sparse matrix solution
```

Figure 35: EQSLV,SPARSE Ansys

The equation that describe the dynamic system of the bladed disk is:

$$[\mathrm{M}]\{\mathrm{x(t)}\} + [\mathrm{C}]\{\mathrm{x(t)}\} + [\mathrm{K}]\{\mathrm{x(t)}\} = \{\mathrm{f_{EXT}(t)}\} + \{\mathrm{f_{NL}(t)}\} \tag{35}$$

where:

1. $x(t)$ is the vector that includes the displacements in the system
2. K is the matrix if stiffness
3. M is the mass matrix
4. C is the viscous damping matrix
5. f_{NL} is a vector that depends on the degree of freedoms (DOFs) constrains
6. f_{EXT} is a vector of excitation forces

The contact iteration between the root of the blade and the disk present a non-linear behaviour as is possible to see form the figure 36.

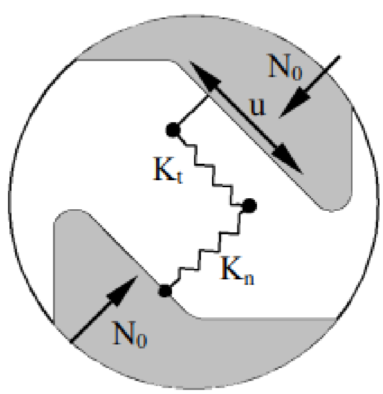

Figure 36: Contact scheme [2]

Solution The blade is excited by an harmonic force and the centrifugal load is applied in two different ways:

1. for the dummy blade (figure 22) a static force is applied in the bottom of the root blade

2. for the bladed disk the real force is calculated because the rotational speed is provided as illustrated in the figure 37

```
OMEGA,0,0,CLBC*pi/30,
```

Figure 37: Rotational speed; CLBC can be setted for different rotational speed of the system. In example $CLBC = 12500rpm$

The static load affects the dynamic system because it increases the stiffness of the system and it influences the pre-load acting on the contact surface. The figure 38 summarize the force on the generic blade contact surface where:

1.
$$\mathrm{T} = \mu \mathrm{N} \tag{36}$$
   T is the tangential force and if is equal to the static friction load the slip occur

2.
$$\mathrm{N} = \frac{\mathrm{F}}{2(\sin\alpha + \mu\cos\alpha)} \tag{37}$$
   is the normal load and F is the static load

In the first part of the solution the script pairs the nodes of the FEM and it fix a local coordinate system with the x axis oriented in the tangential force direction. With this local coordinate system is possible to evaluate the displacements among the two directions N and T. Once the forces act on the contact surfaces the elements are assumed with a low

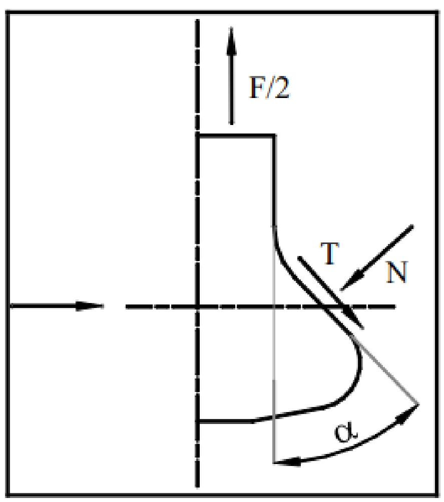

Figure 38: Scheme of the contact forces [2]

penetration, almost impenetrable, in order to increase the stability of the calculation. The CONTA175 and TARGE170 functions, provided by Ansys mechanical library command, are used.

1. CONTA175: this command is used in combination of the TARGE170 command to represent contact and sliding between two surfaces. The main different between

CONTA175 and CONTA174, used in [2], is a different specification of the contact element. In the first one the contact element are two bodies and in the second, used in this thesis, are two surfaces. This commando is useful because it supports

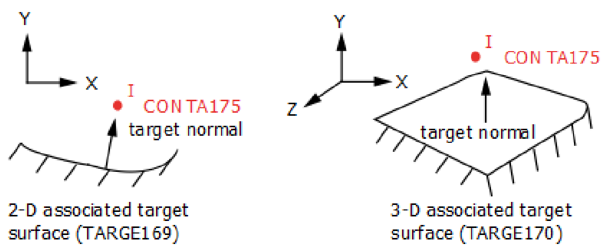

Figure 39: Figure 175.1: CONTA175 Geometry, Ansys 18 Library

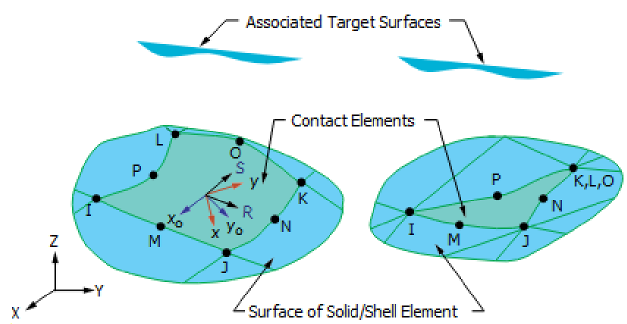

Figure 40: Figure 174.1: CONTA174 Geometry, Ansys 18 Library

isotropic and orthotropic Coulomb friction.

2. TARGE170: the contact between two bodies occurs when the target surface penetrates the element surface and those surfaces are defined by the target command. TARGE170 associated with the command above identify a surfaces defined by 3 nodes the normal vector of the surface is coupled to one node of the other contact surface.

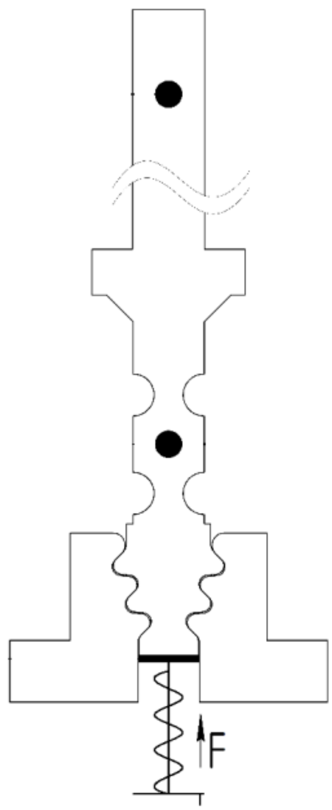

Figure 41: Dummy blade set-up scheme

2.1.2 Numerical method

In order to investigate how the friction between two elements affects damping different experimental results ([3],[29]) are provided. Those experimental results are useful in order to clarify if the script based in the analytical equations already explained works. An explanation of the script structure is provided, experimental and numerical results are compared.

Structure of the program The architecture of the script used is described in the figure 42. The language of the script is Ansys based and Ansys Mechanical is used in order to perform the numerical task. In the inizialization section different parameters are inserted

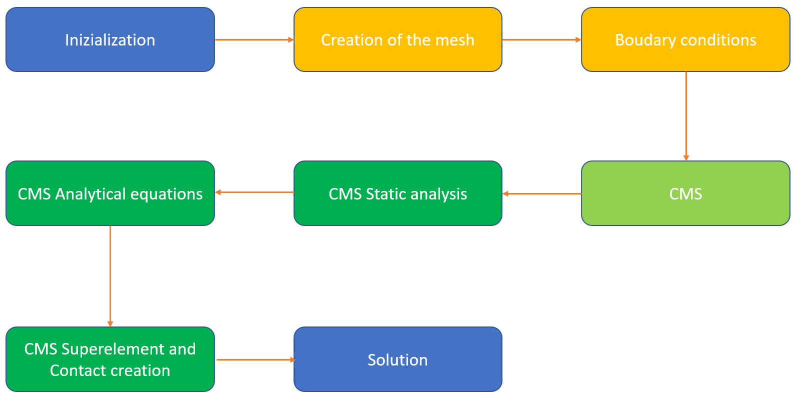

Figure 42: Script diagram

such as:

1. friction coefficient (FC), in case of contact iteration between two metal bodies the coefficient is assumed from 0.15 to 0.7

2. pinb (Pinball radius), this parameter is needed to pair the contact surfaces

3. PTOL (Penetration tolerance), is assumed equal to 1 in order to simplify the calculations and do not take in account the penetration of the bodies during the calculation

4. Force, is the value of the force response and can vary form 10 N to 100 N depending on the stiffness of the system under study

5. PRForce (Pressure Force), is essentially the simulation of the centrifugal load as already described. In the sector of disk and in the complete disk this parameter is not considered because the real centrifugal force is calculated with the following parameter

6. CLBC, is the rotational speed of the element

7. dmprbeta, is the constant of global damping and is assumed as 0.00141 from the experimental data

8. nu (Poisson coefficient), is 0.34

9. E1,E2 (Elastic modulus), both elastic modulus are assumed equal and for the dummy blade are 1.77e11 and for the sector of the disk (figure 43), disk complete are 1.18e11

10. DENS (density), is 4510 for the sector of the disk and the complete disk and 7850 for the dummy blade. Is assumed the density is equal in the blade and in the disk. Than both contact surfaces have the same material properties.

The advantage of the structure showed in the figure 42 is the flexibility because is possible to modify and test every block separately from the others.
In the creation of the mesh the parasolid file is loaded and the mesh parameters are inserted. The creation of the mesh is done in two different parts:

1. loading of the parasolid file and creation of the general mesh

2. mesh refinement focusing on the contact surfaces, load affected zones and areas of interest

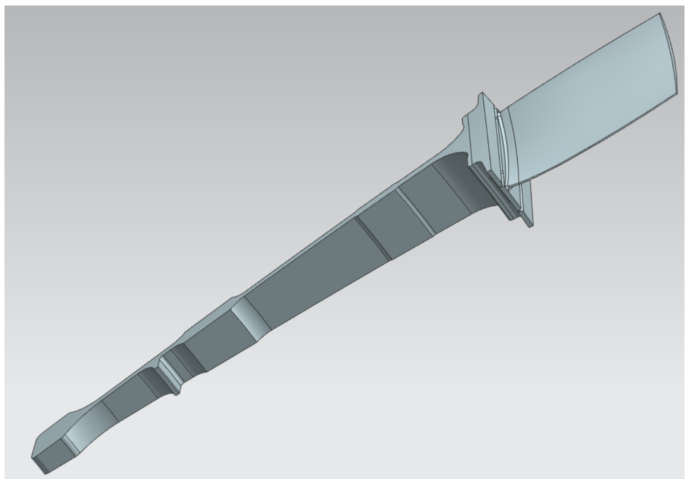

Figure 43: Parasolid of the section of the disk model

The mesh near the contact zones have a particular interest because the pressure gradients are high and in order to produce reliable results a particular attention must be done. In the figure 44 is possible to see an extract of the mesh script. In this case different lines in the contact section are selected and divided in 8 segment. The script showed in the figure 44 is useful in order to produce a regular and controlled mesh in the contact surfaces In

```
FLST,5,8,4,ORDE,8
FITEM,5,3
FITEM,5,134
FITEM,5,4
FITEM,5,137
FITEM,5,2
FITEM,5,140
FITEM,5,1
FITEM,5,143
CM,_Y,LINE
LSEL, , , ,P51X
CM,_Y1,LINE
CMSEL,,_Y
!*
LESIZE,_Y1, , ,8, , , , ,1
```

Figure 44: Mesh script section

this section the nodes where the vibration amplitude is measured are localized and they are located in the shroud of the blade. The location of the nodes through the intersection of areas in the 3 directions can cause some problems during the process if the mesh is very fine, but as is proved in [15] after a certain value the error of the calculation due the mesh size can be negligible. Under this assumption the mesh size is chose in order to have the

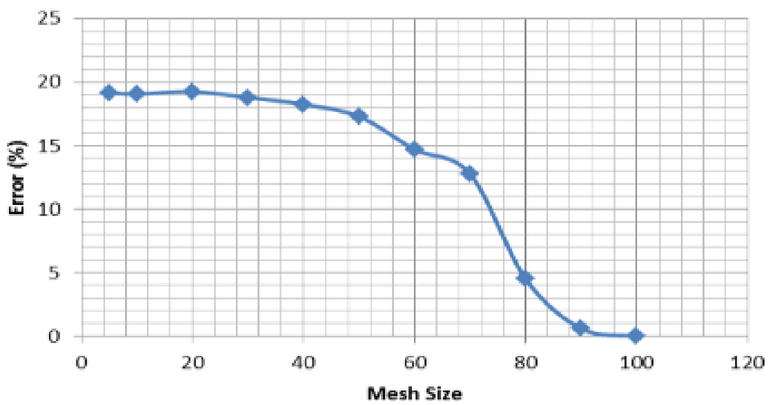

Figure 45: Mesh error described in [15]

best results considering the performance of the laptop used for the simulation with the following specification: Intel core i7 2.50GHz, 8GB ram memory. The size of the mesh and the number of the contact elements affects the simulation and those parameters are dimensioned in order to perform an in-core memory calculation.
In the boundary condition script the model is oriented in the right direction and the reference systems in the contact nodes are created in order to calculate the horizontal and vertical displacement as explained in the theory. The contact surface is created.
The CMS script is divided in 4 parts in the order indicated in the figure 42 because every section can be tested separately, however for the final calculation all the sections must be solved.
In the CMS Static analysis the structural analysis in every point of contact is performed. The number of contacts, num_cont in the figure 46, are calculated in the previous section and as is explained in the theory the normal pressure, normal penetration and the slide force are calculated in the contact node reference system.

```
etable,norpene,cont, pene
!*
*vmask,emask%i%(1)
*vget,uz_par_all%i%(1,1),elem,,etab,norpene
!*
*vmask,emask%i%(1)
*vfun,uz_par%i%(1,1),comp,uz_par_all%i%(1,1)
!*

*VSCFUN, D_%i%, mean, uz_par%i%(1,1)
```

Figure 46: CMS Static analysis script section

In the CMS Analytical equations the analytical equation described in the theory are performed such as the pressure distribution or the tangential stiffness.
In the CMS Super-element and Contact creation the modal analysis is performed and the superelemnt is created. The command MATRIX27 is used because the kinematic response is defined by the stiffness of the element and damping. As is possible to see in the figure

47 the matrix created by the command relates two nodes with 6 degree of freedom (3 for the rotation and 3 for the translation). For this thesis every system is transformed to a super-element because it has a reduced number of degree of freedom compared to the full model and the precision of the calculations is guaranteed. In case of the complete disk two

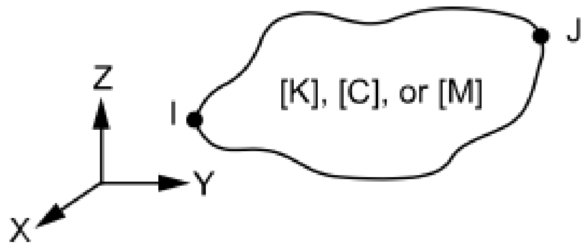

Figure 47: Figure 27.1: MATRIX27 Schematic, Ansys 18 Library

ways could be possible using the sector of the disk model (figure 43):

1. create a complete model revolving the mesh

2. create a complete model revolving the superelement

The second way is used because it requires a much smaller amount of memory for the calculation considering that the contact problem produce a non-linear behaviour.
In the Solution in the case of the complete disk the nodes of two adjacent super-elements are paired. The same procedure is adopted for the contact regions because every super-element must be provided of the contact region between the root of the blade and the disk in order to produce a real result. In this section the vibration amplitude of the blade is calculated for a certain range of values that are inserted in the previous part of the script. In this section of the program the hysteresis cycle is created and the dissipation of energy calculated as showed in the figure 48. This part of the thesis is fundamental in

```
*do,N_RAS_i,1,dQ+1,
*SET,PAR_l_int(N_RAS_i,0),DX%nstat%(N_RAS_i,2)
*SET,PAR_l_int(N_RAS_i,1),DX%nstat%(N_RAS_i,1)
*enddo

*VITRP, ParR_I(1), PAR_l_int(1,1), ParI(1),,

DXe=ParI(1)

*if,DXe,le,DX%nstat%(dQ+1,2),then
Qs=ParR_I(1)
DXs=DXe
*else
Qs=DX%nstat%(dQ+1,1)
DXs=DX%nstat%(dQ+1,2)
*endif
```

Figure 48: CMS Solution script section

order to analyse how the contact surfaces affect the amplitude of the vibration. In this section of the script the tangential and normal stiffness are evaluated in order to create the hysteresis diagram. An output file is produced with the structure indicated in the table 1. The output file is divided in four columns. Here the columns are described from the first to the last:

1. amplitude in terms of acceleration

2. frequency in Hz

0,0000331288	187,70	1,00	0,0002145418
0,0000557646	188,00	1,00	0,0005630497
0,0000486347	188,30	8,00	0,0008241300
0,0000437484	188,60	1,00	0,0002361015
0,0000490880	188,32	16,00	0,0003037497
0,0000588346	188,44	1,00	0,0009559164
0,0000470527	188,56	1,00	0,0002798876
0,0000381023	188,68	1,00	0,0001677268
0,0000316209	188,80	1,00	0,0001035249

Table 1: CMS Solution output file

3. number of iteration, is possible to set a maximum number of iteration in order to stop the calculation if the solution does not converge

4. difference ΔE between two iterations

The calculation of the amplitude for a certain value of the frequency is stopped if the numbers of iterations exceed the maximum or if the gap between two values fulfils the relation 38.

$$\Delta E = \frac{A_i - A_{i+1}}{A_i} < 0.001 \tag{38}$$

The output file is the result of the procedure explained in the figure 42 and is noticeable that if the behaviour of the system is non-linear more iterations are performed in order to achieve the correct precision of the calculation. Using the output file is possible to plot the graph showed in the figure 49. In the vertical axis the amplitude response and in the horizontal one the frequency are plotted for different pre-loads, if the model is the dummy blade, or rotational speeds. The amplitude is obtained multiplying the first and the second column of the output file: $(2\pi frquency)^2 amplitude$.

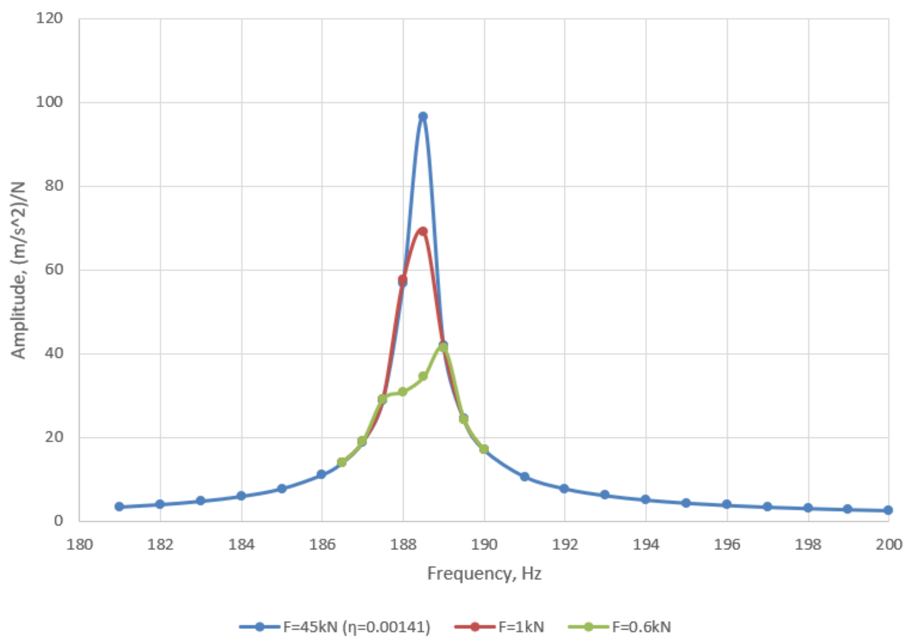

Figure 49: Amplitude/Frequency example for different static loads

2.2 Model and Mesh

In the figure 50 the parasolid file of the dummy bladed is showed. Is noticeable that the blade has a three tree root and the base is assumed as an extreme rigid structure. The static force F that simulates the centrifugal force is applied in the flat surface in the bottom of the root of the blade. The system is tested for various values of the static force and for

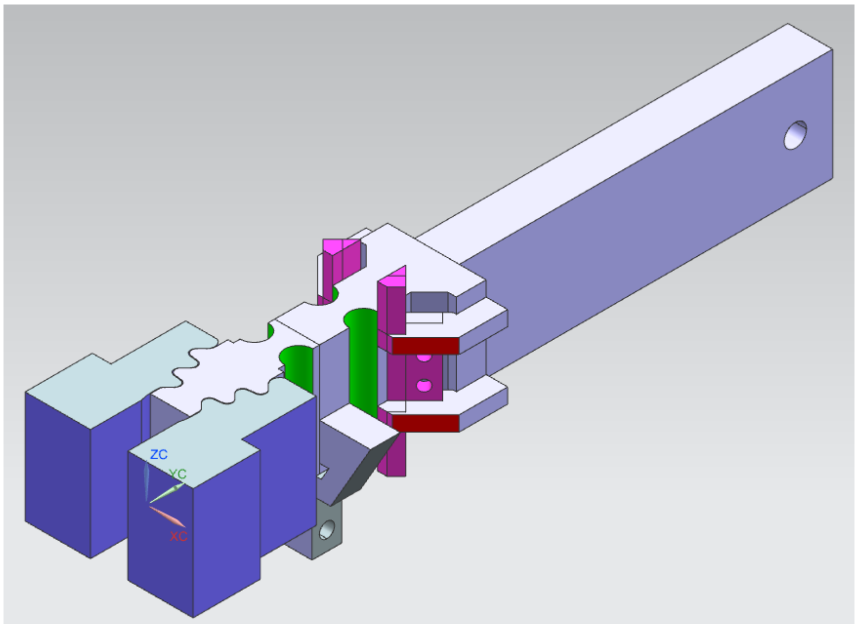

Figure 50: Parasolid dummyblade

different values of the friction coefficient f.
Particular attention is made in the contact region as is possible to see in the figure 51 where the mesh is fine and the region is divided into regular rectangles in order to increase the efficiency of the TARGE170 command. In the figure 52 is showed the mesh in the root blade contact surface. The same mesh topology is reflected in the disk, or in the base in case of dummy bade in order to pair each node.

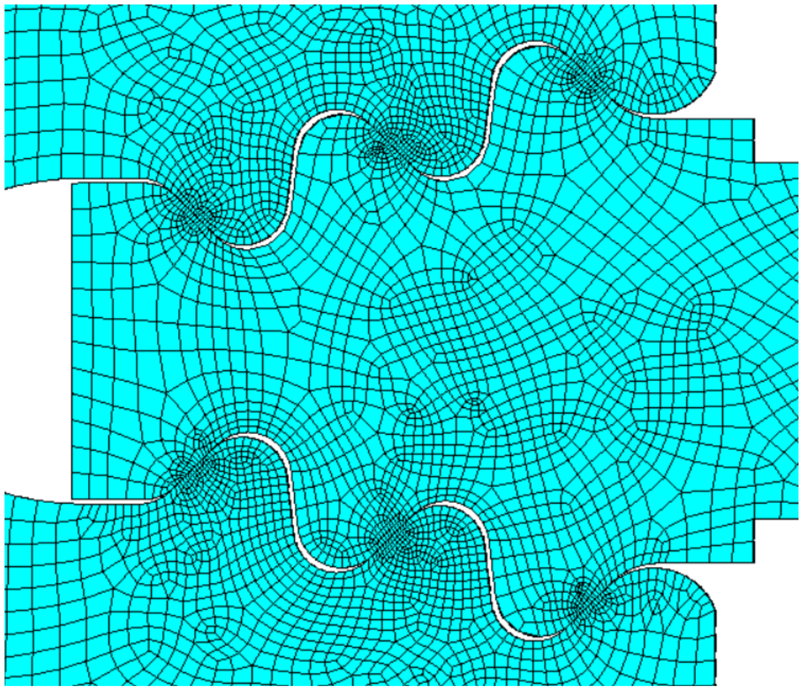

Figure 51: Dummy blade mesh detail

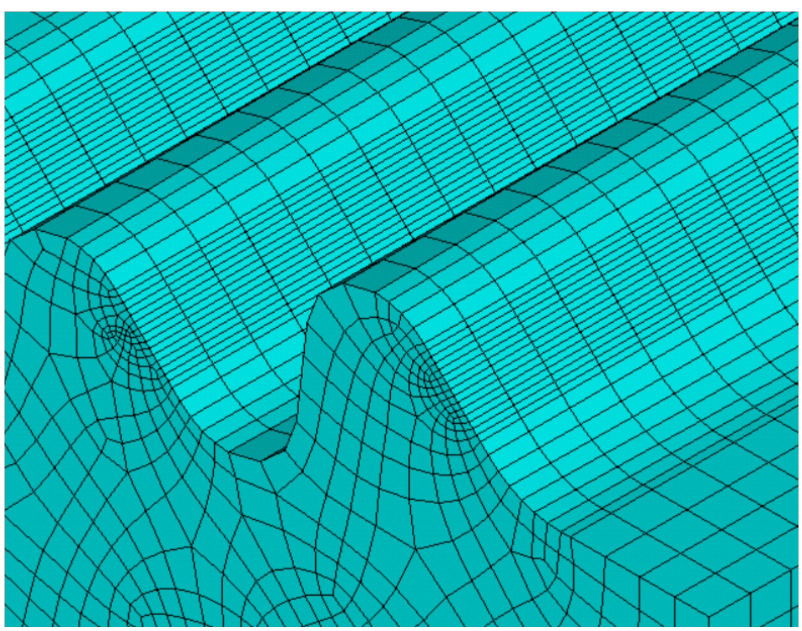

Figure 52: Dummy blade mesh blade/disk contact region

2.3 Data

In this section the experimental data provided in [3] and [29] are compared with the numerical data. The data are explained through graphs in order to improve the reading of the thesis.

f=0.15 The experimental data are showed in the figure 53. Assuming the experimental

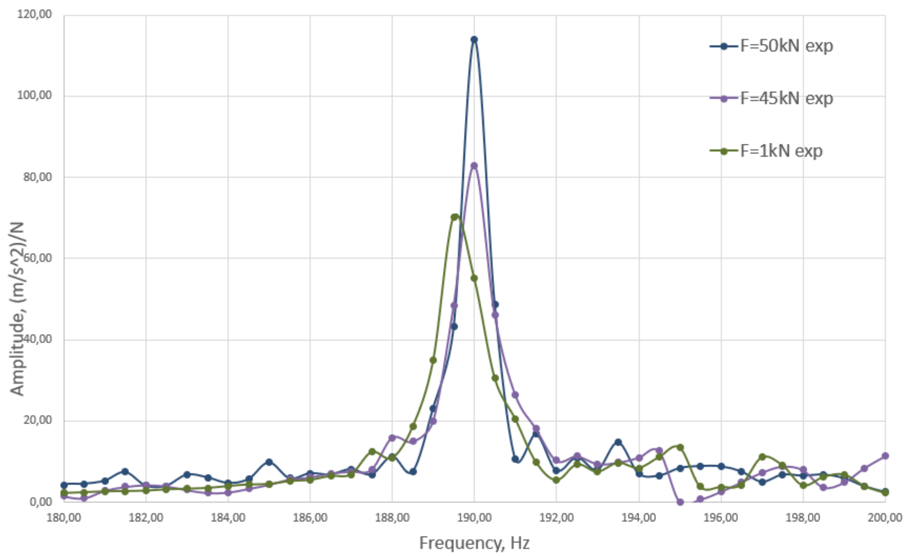

Figure 53: Experimental data. f=0.15

data as correct is possible to notice that the pick is at 190Hz and decreasing the value of F the pick moves left and the amplitude decrease. In the figure 54 the numerical data are presented. Is possible to notice that:

1. the pick moves 1.5 Hz left
2. the maximum amplitude value is similar
3. damping occurs

Focusing on the damping abilities of the contact surfaces the smooth of the vibration exist for low values of the static force F which are correlated to low centrifugal forces. As is possible to notice in the figure 54 the damping occurs until F=2 kN, for F=3 kN the damping value start to become is negligible. After F=3 kN all the amplitude-frequency curves overlap as showed in the figure 55. Experimental and numerical data are compared in the figure 55 and only relevant plots are showed.

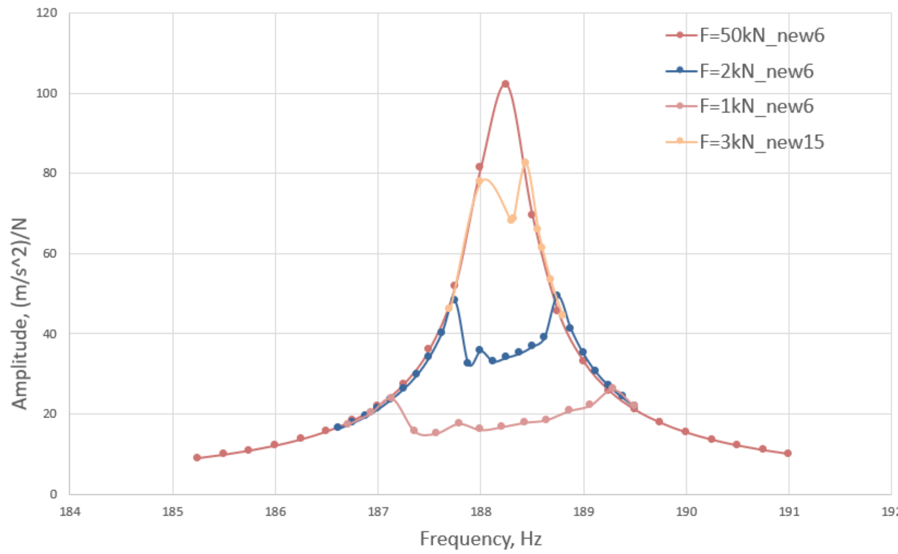

Figure 54: Numerical data data. f=0.15

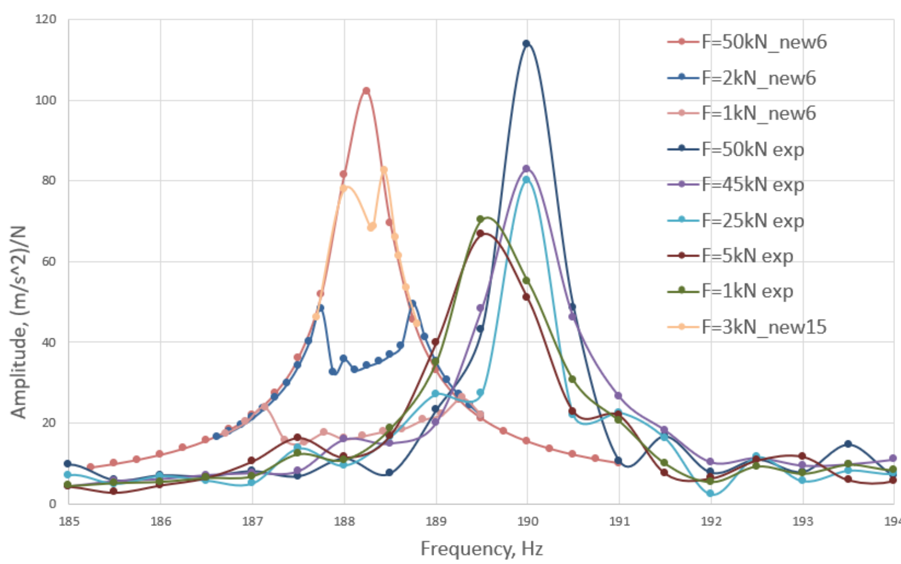

Figure 55: Numerical and Experimental data data. f=0.15

f=0.3 The experimental data are showed in the figure 56. Comparing the experimental data with the previous one is possible to notice that the amplitude and position of the pick remain the same. In the figure 57 the numerical data are showed and is possible to notice

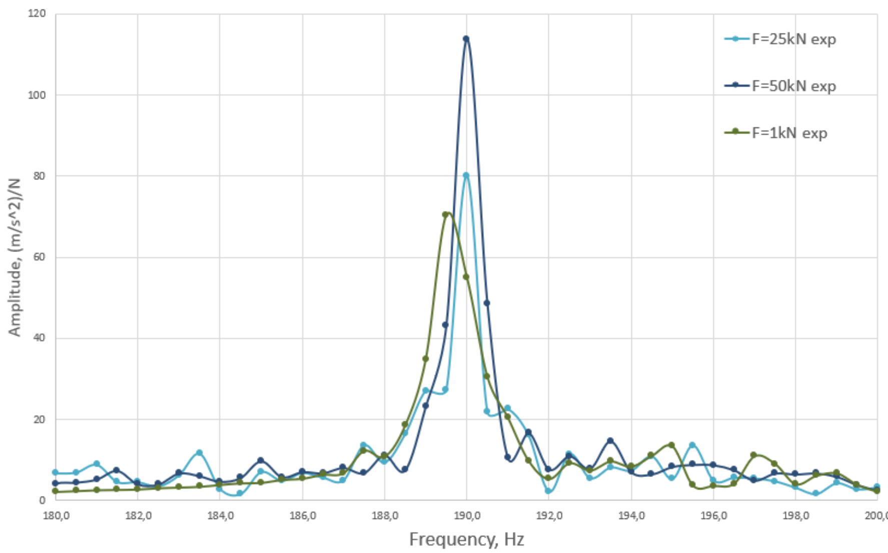

Figure 56: Experimental data. f=0.30

that the damping of the vibrations present a different characteristic. The friction coefficient affects the damping abilities of the contact surfaces and increasing f the dumbing abilities decrease. In the figure 58 the numerical data and experimental data are compared and the

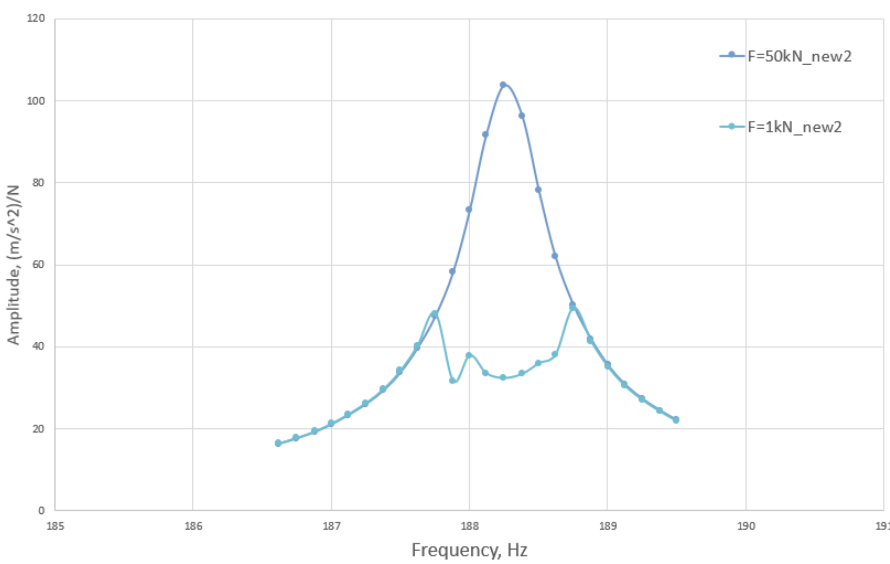

Figure 57: Numerical data. f=0.30

numerical calculation shows that only for F=1 kN the damping occur.

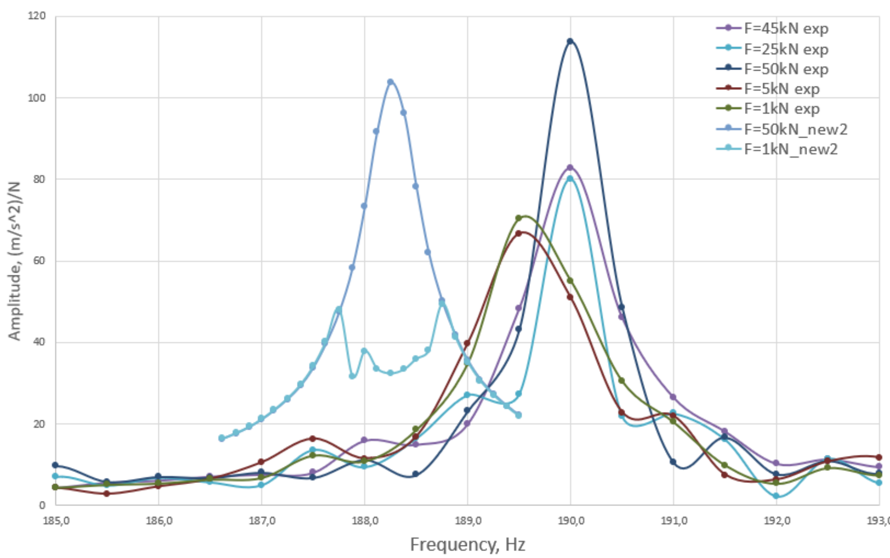

Figure 58: Numerical and Experimental data. f=0.30

f=0.5 The experimental data are showed in the figure 59. As is possible to notice from

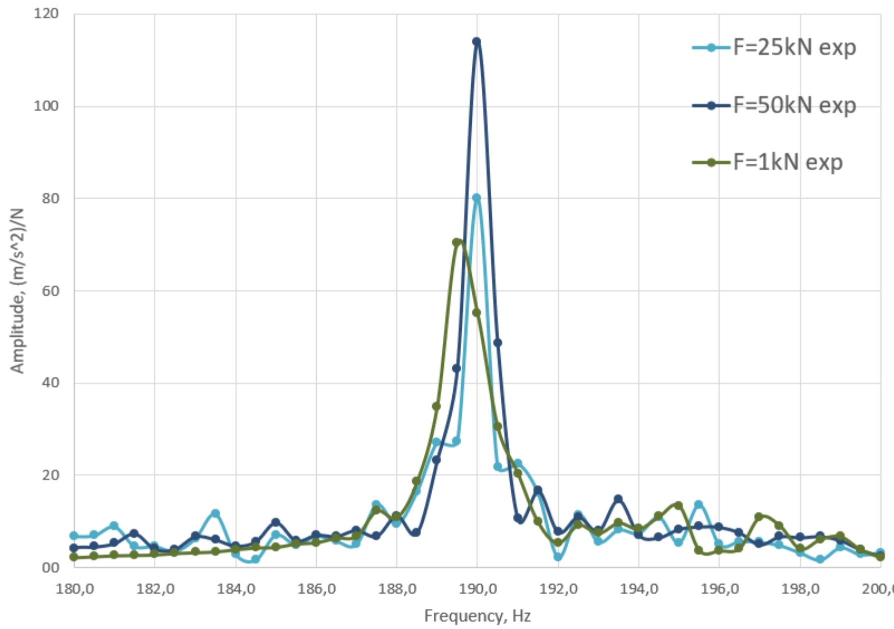

Figure 59: Experimental data. f=0.50

the figure 60 the amplitude of the pick decrease and a new value of F=0.6 kN is investigated. The damping occurs for F=1 kN and F=0.6 kN. In the figure 61 numerical and experimental data are compared.

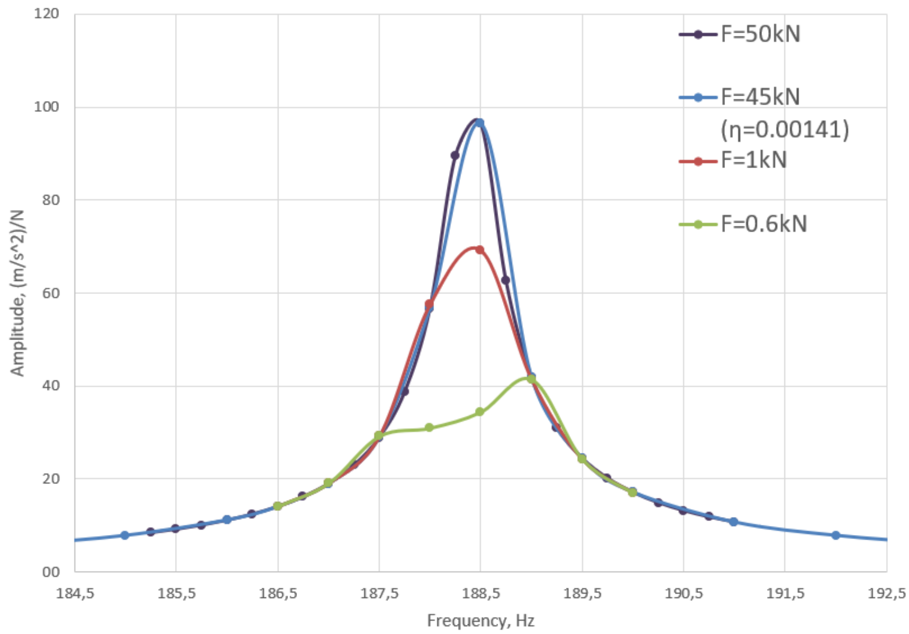

Figure 60: Numerical data. f=0.50

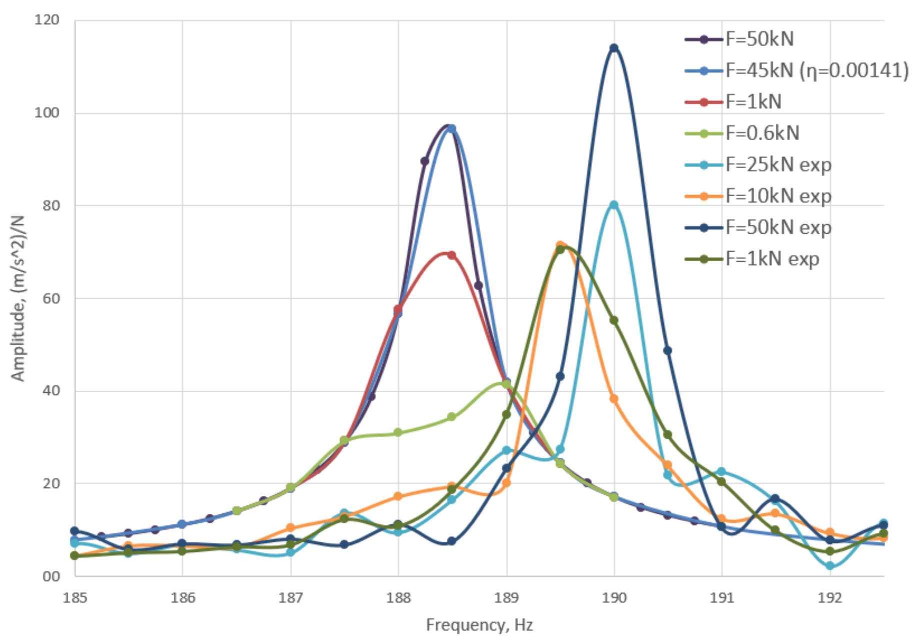

Figure 61: Numerical and Experimental data. f=0.50

f=0.7 The experimental data are showed in the figure 62 and the result obtained are similar of f=0.5. This case confirm that increasing the friction coefficient the damping

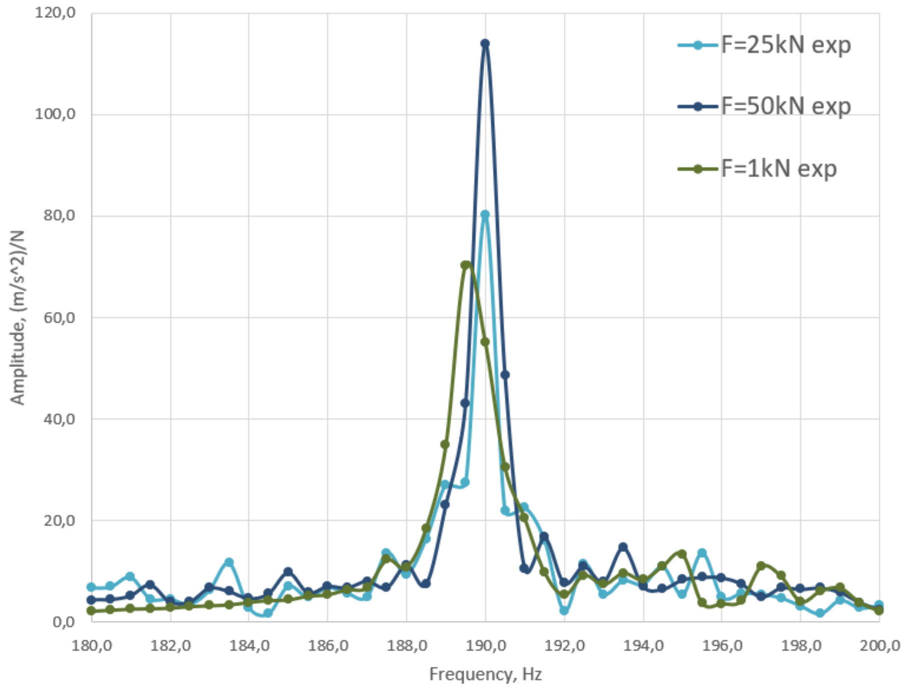

Figure 62: Experimental data. f=0.70

abilities of the contact surface decrease and as is possible to see in the figure 63 damping occurs only for F=0.4 kN. In the figure 64 numerical and experimental data are compared.

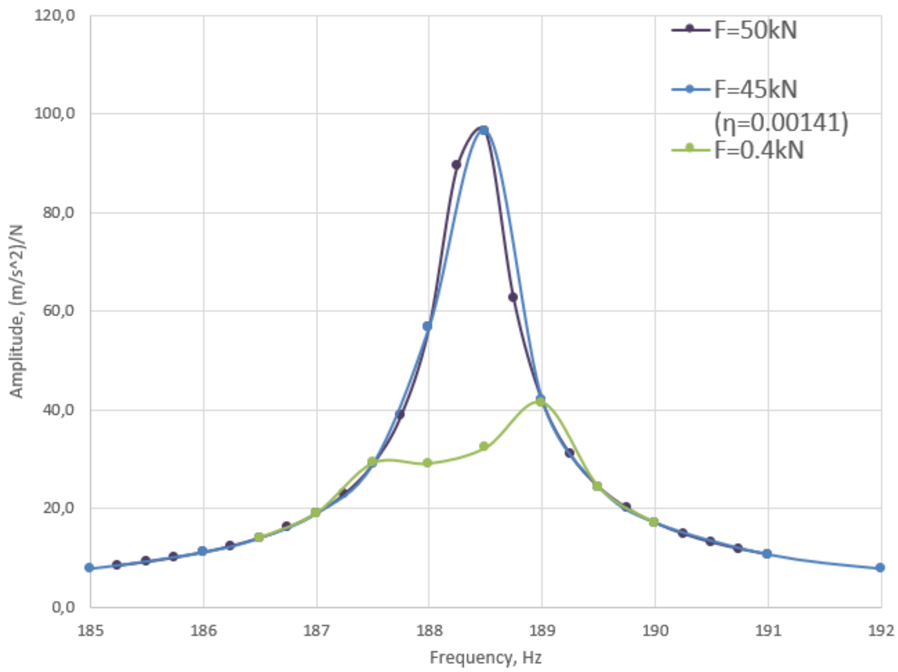

Figure 63: Numerical data. f=0.70

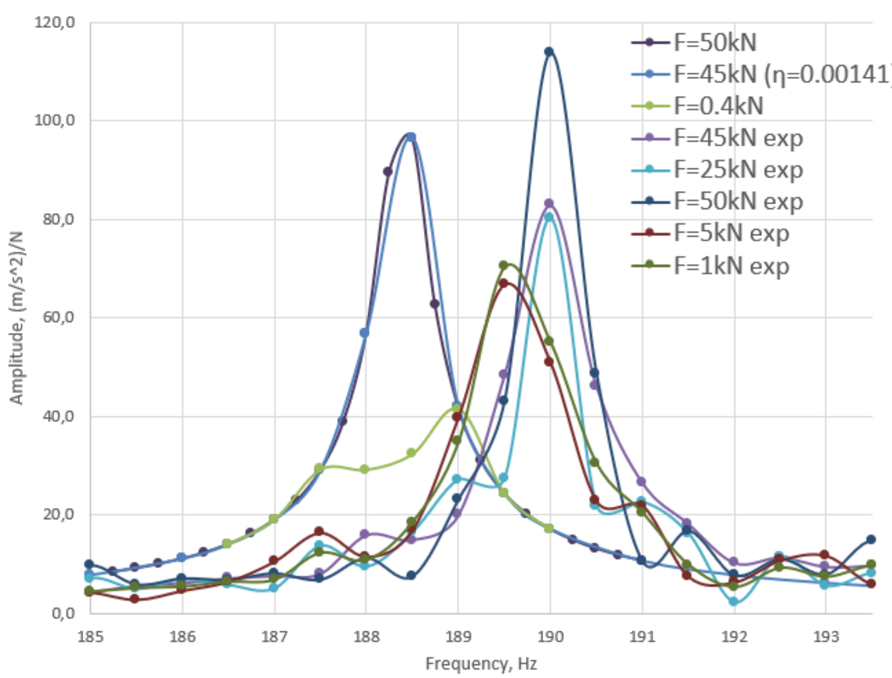

Figure 64: Numerical and Experimental data. f=0.70

3 Section of bladed disk

In this section the mesh and the numerical calculation of the model sector of the disk is presented. The model respect the real dimensions of a NK family compressor blade and the model is showed in the figure 43. The complete disk present in the next section presents 73 blades and in this chapter the analysis of only one sector is presented. For the analysis the same code of the dummy blade is used because the precision of the results produced is proved comparing the numerical and experimental result. The difference between the code used in the dummy blade chapter and in the section of bladed disk is that the centrifugal force is calculated consider the rotational speed of the model. The static pre-load force F is not setted, but is calculated considering as input the rotational speed of the engine and the material properties data.

3.1 Model and Mesh

The model is a section of the NK family engine high pressure compressor. The blade present a dovetail connection to the disk as is possible to see in the figure 66 and compared to the dummy blade the model present a realistic geometry of the blade as showed in the figure 65. The blade is connected to the disk thanks to a dovetail root as showed in the

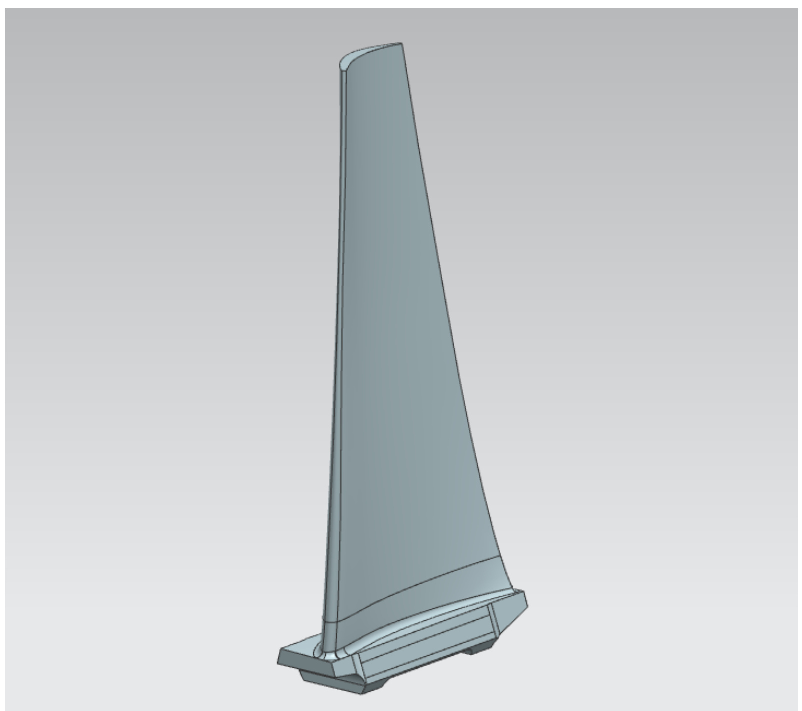

Figure 65: Blade detail, sector of the disk

figure 66 and the sides of the dovetail are in contact to the disk. The mesh of the model is showed in the figure 67 and the contact surfaces are meshed using the same methodology of the dummy blade. In the contact region between the blade and the disk the mesh is regular and the size of the elements is setted using vertical and horizontal number of divisions. For the lower part of the disk and the upper part of the blade a swept mesh methodology is used.

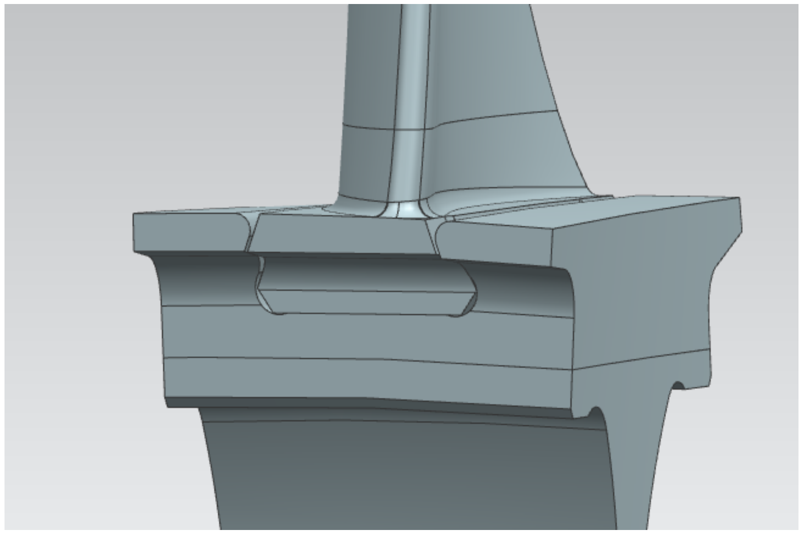

Figure 66: Dovetail detail, sector of the disk

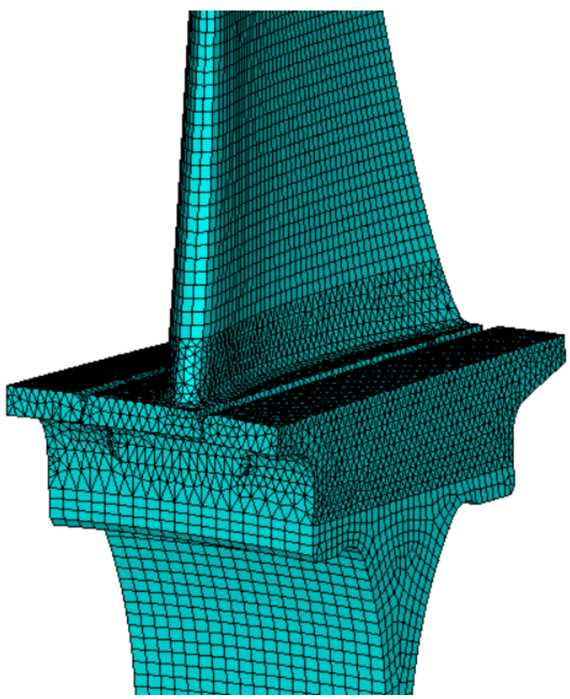

Figure 67: Mesh, sector of the disk

3.2 Data

As in the dummy blade different values of friction coefficient and centrifugal forces are considered. The centrifugal force is not statical but it is calculated from the script in fact the data are presented for various rotational speeds.

f=0.15 The numerical data are showed in the figure 68. From the dummy blade section some behaviours such as:

1. increasing the friction coefficient f the damping abilities in the contact surfaces decrease
2. from the experimental data increasing the stiffness of the system, changing the value of the static force F, moves the pick of the frequency to the right
3. the damping behaviour is less noticeable for high centrifugal force values

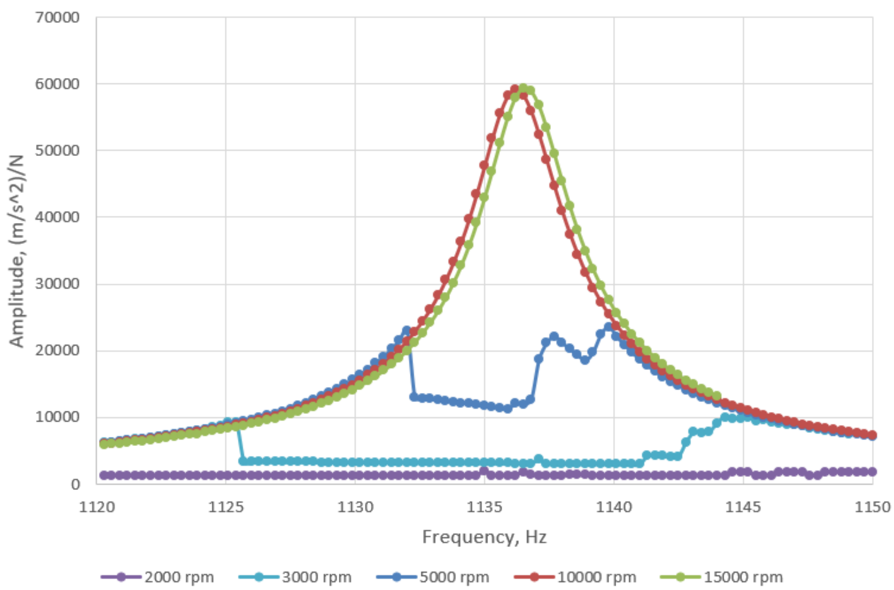

Figure 68: Numerical data. f=0.15

From the figure 68 this behaviours are showed. Comparing the 10000 rpm and 15000 rpm lines is noticeable that the pick of amplitude moves right. This behaviour can be explained with the increasing of the stiffness level of system related to the increase of the centrifugal force. The damping performance of the root of the blade are visible until 5000 rpm, however is possible to assume that there is an intermediate curve before 10000 rpm values. The 2000 rpm curve shows an interesting damping behaviour, however the gas turbine engine pass the 2000 rpm regime very fast and this rotational speed is excluded in the idle regime of rotation. Under this consideration the first interesting curve is the 3000 rpm.

f=0.30 The numerical data are showed in the figure 69. Increasing the friction coefficient is possible to notice that the damping effect decrease and in 5000 rpm can be considered as the last rotational speed where the damping occurs. The position and the amplitude of the pick are stable.

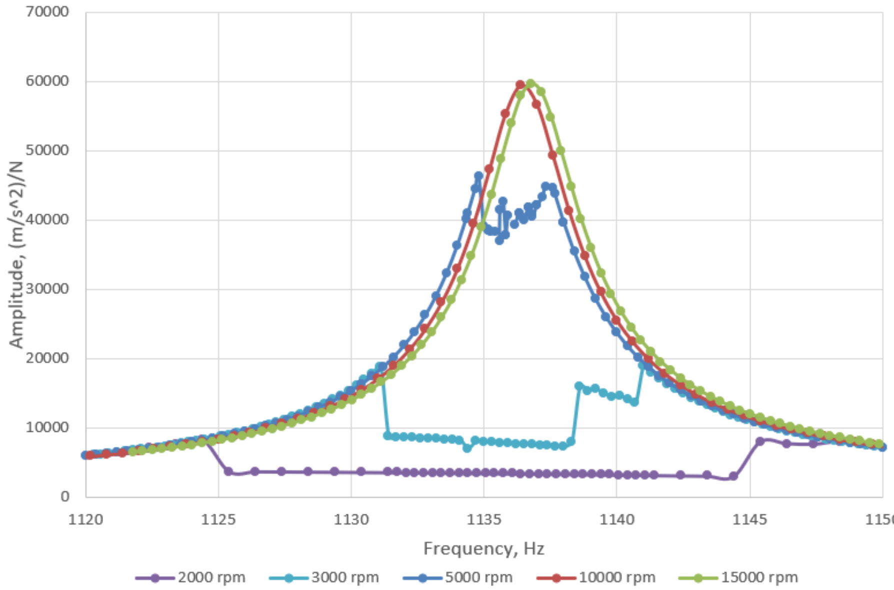

Figure 69: Numerical data. f=0.30

f=0.70 The numerical data are showed in the figure 70. The damping behaviour exist only for low rotational speed. Comparing the graph of f=0.70 with the graph above for the sector of the disk is possible to confirm that the damping abilities are more effective for lower friction coefficient.

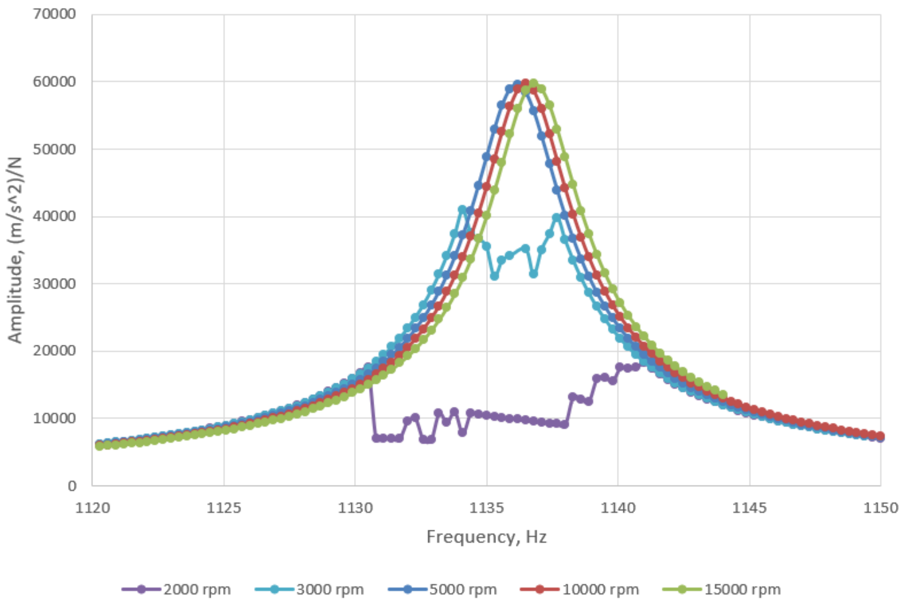

Figure 70: Numerical data. f=0.70

4 Bladed disk

In this section the section of bladed disk is used in order to create the complete bladed disk with 73 blades. The numerical calculations are performed taking in account that the big amount of data should be manipulated using a high performance calculator, for this thesis a laptop with 8Gb of ram and Intel i7 2.5GHz processor is used. However a numerical method is provided and the calculations performed.

4.1 Model and Mesh

In the figure 71 the mesh of the sector of the disk is showed and is noticeable, comparing with the figure 67, that the size of the elements is increased. This choice derives from the computational power of the laptop used for the simulations. In order to build the

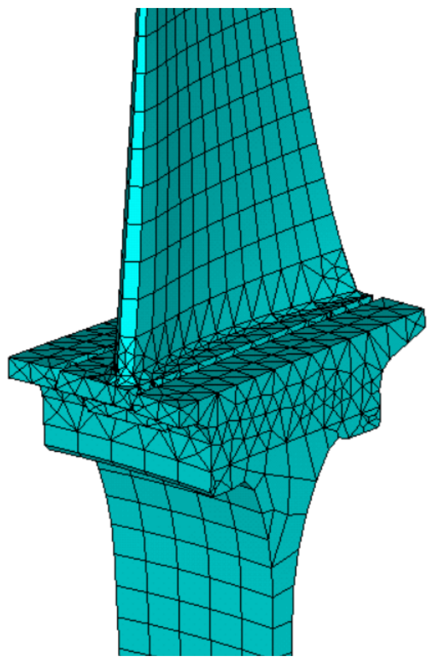

Figure 71: Mesh, bladed disk

complete bladed disk with 73 blades the left and the right side of the sector of the disk present the same topology. The sector of the disk with the same side topology presents the same mesh and this clarification is needed to pair two adjacent super-elements and share the side nodes in order to transfer the dynamic and static loads. In the figure 72 the black arrow indicates the common-side region between two sectors and is possible to observe that the elements are paired. In the figure 77 and figure 73 the complete mesh of the model is showed.

4.2 Data

In this section the complete disk with 73 blades is considered. The model requires a long calculation as described above and is tested for a singular rotational speed and friction coefficient in the contact sections.

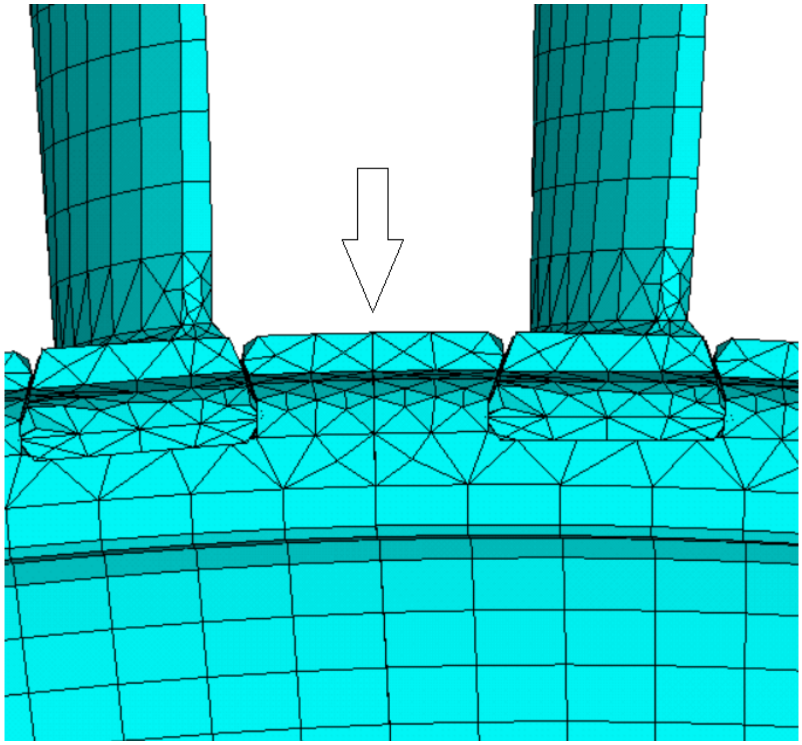

Figure 72: Share mesh, bladed disk

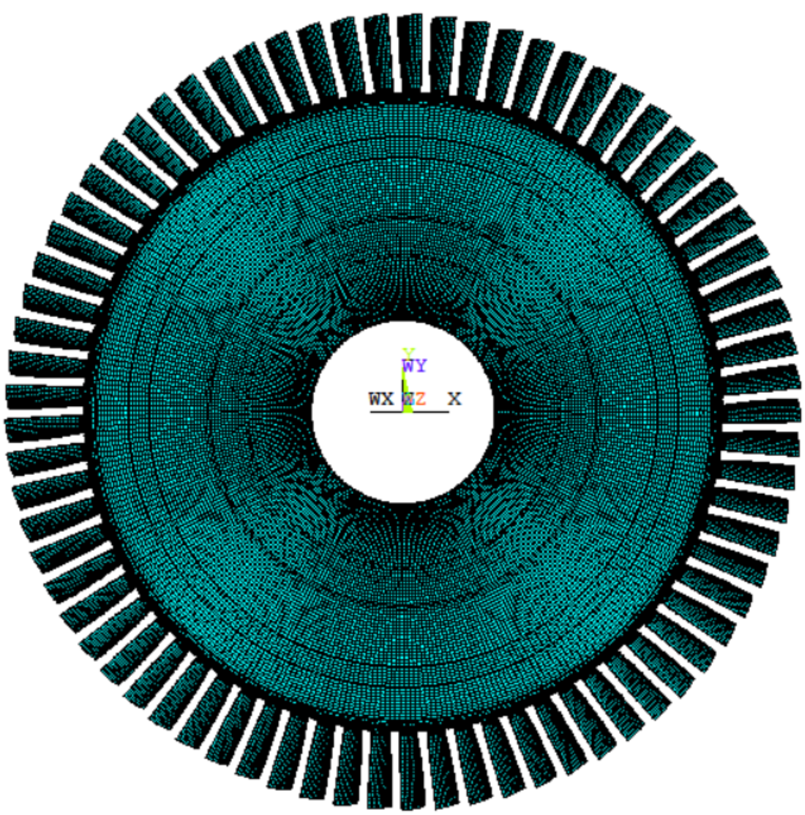

Figure 73: Mesh, bladed disk

f=0.3 ; 12000rpm The numerical data are showed in the figure 74.

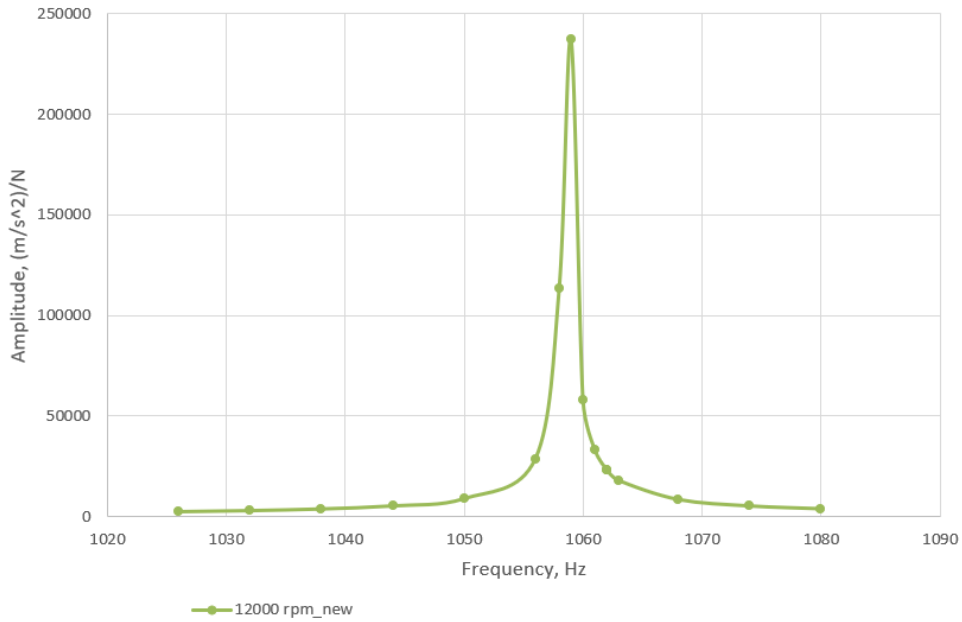

Figure 74: Numerical data

The data showed in the figure 74 refer to the blade number 1 identified from the positive x axis in the figure 73. However is possible to notice that the script analyse the first mode shape, called umbrella shape. That deduction is based on the data produced for the others 72 blades of the model. Every blade have the same amplitude, except a negligible different due errors, as proved in the tables in the appendix section. The figure 75 shows this behaviour for the bladed disk.
Due the amount of time involved for the calculation the bladed disk behaviour is simulated only for one range of rotational speed assuming that the contact behaviours are similar to the sector of the disk section.

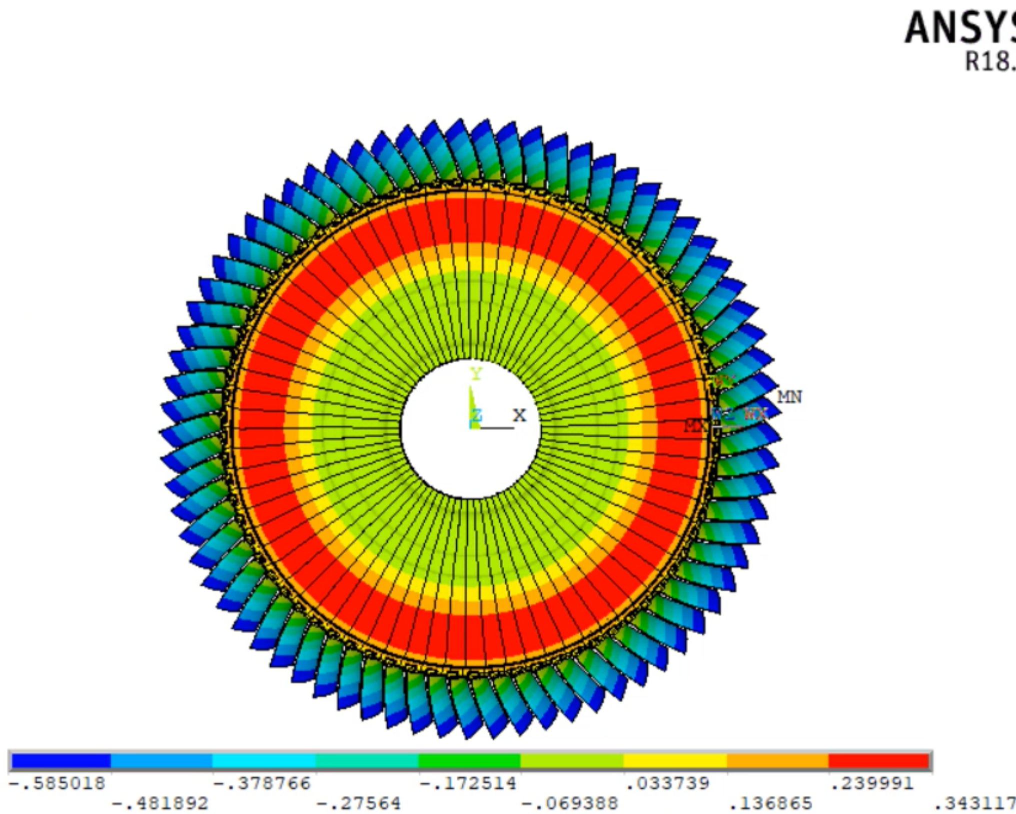

Figure 75: Umbrella mode shape

5 Conclusions

Dummy blade

1. Decreasing the mesh size and increasing the number of contact nodes do not affect the numerical calculation. As is possible to see in the figure 76 increasing the number of contacts from 6 to 24 nodes along the minor segment in the tree shape root of the blade.

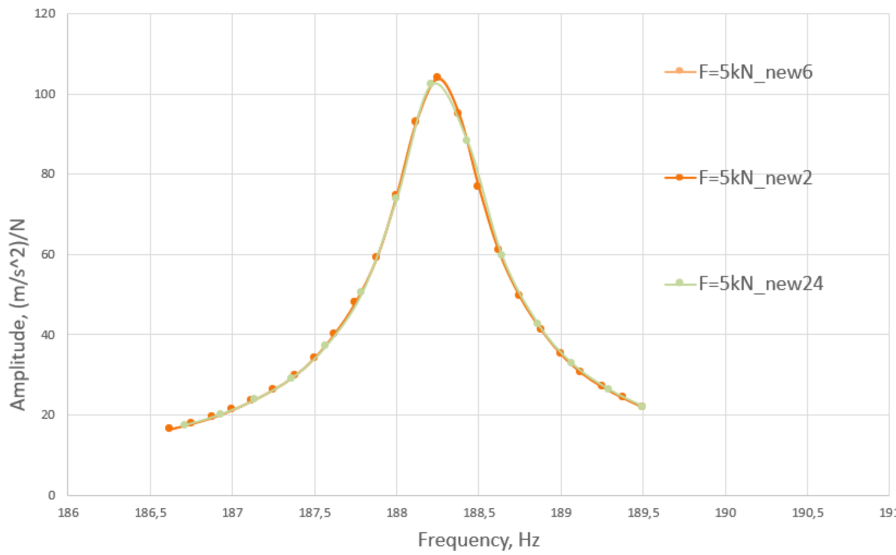

Figure 76: Mesh size numerical comparison in dummy blade

2. The numerical model described in this thesis using Ansys can be assumed as correct due the comparison of the numerical and experimental data. Considering the assumptions described in the theory of the model section the position of the pick differers less than 1% and the amplitude of the pick is satisfiable as is possible to see in the figure 55 or figure 58 of figure 61

Section of the disk The numerical model tested in the dummy blade section is applied to the sector of the disk model. Considering the conclusions of the dummy blade section is possible to assume the numerical data of the sector of the disk as correct. Some behaviours observed in the dummy blade section are noticed in this section such as:

1. the damping abilities of the contact surfaces in the blade are noticeable for low rotational speed. Considering the figure 69 the damping behaviour is effective until 5000 rpm and the coefficient f is equal to 0.30.

2. the damping abilities of the contact surfaces in the blade decreases if the friction coefficient increase. This conclusion is widely know by the literature.

Bladed disk Observing the figure 74 some considerations can be done considering the mesh size of the elements in the contact surfaces and the non-linear behaviour of the contact iterations.

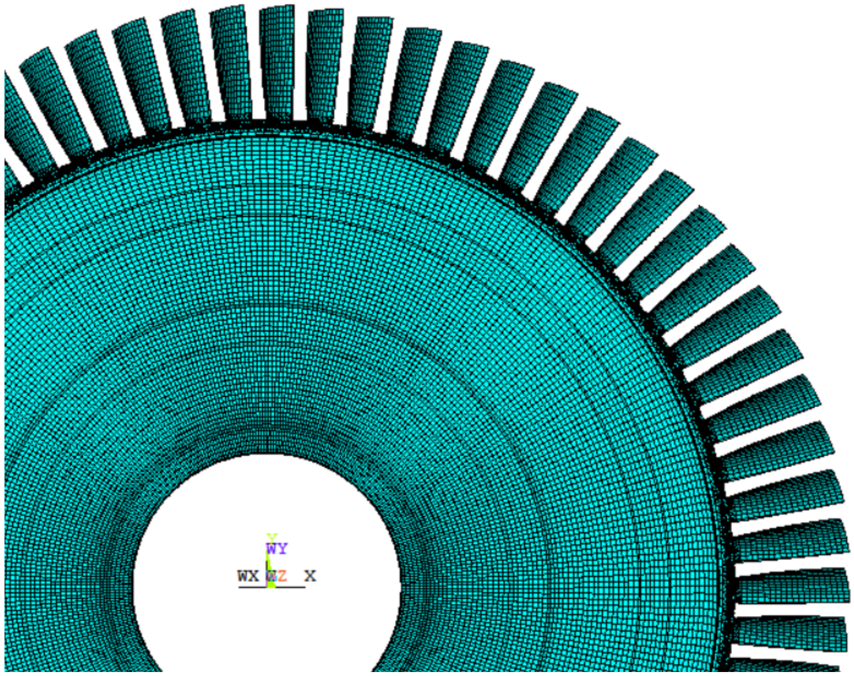

Figure 77: Mesh, bladed disk

1. in the figure 74 the numerical data of the calculation are showed. Is possible to notice that the bladed disk behave like the sector of the disk. Is possible to assume the left and right part of the curve as correct, however the mesh size strongly influences the calculations near the maximum amplitude frequency.

2. in the figure 78 the numerical data of the disk and the sector of the disk are compared. Comparing the wideness of the frequency range the bladed disk presents the same wideness of the sector of the disk, that means the script works correctly. Comparing the rage of frequencies involved in the calculations is possible to notice that the position of the pick differs about 80 Hz. Considering the precision of the calculation due the mesh size of the bladed disk this result is positive for a future development of the model because it ensure that the script works correctly.

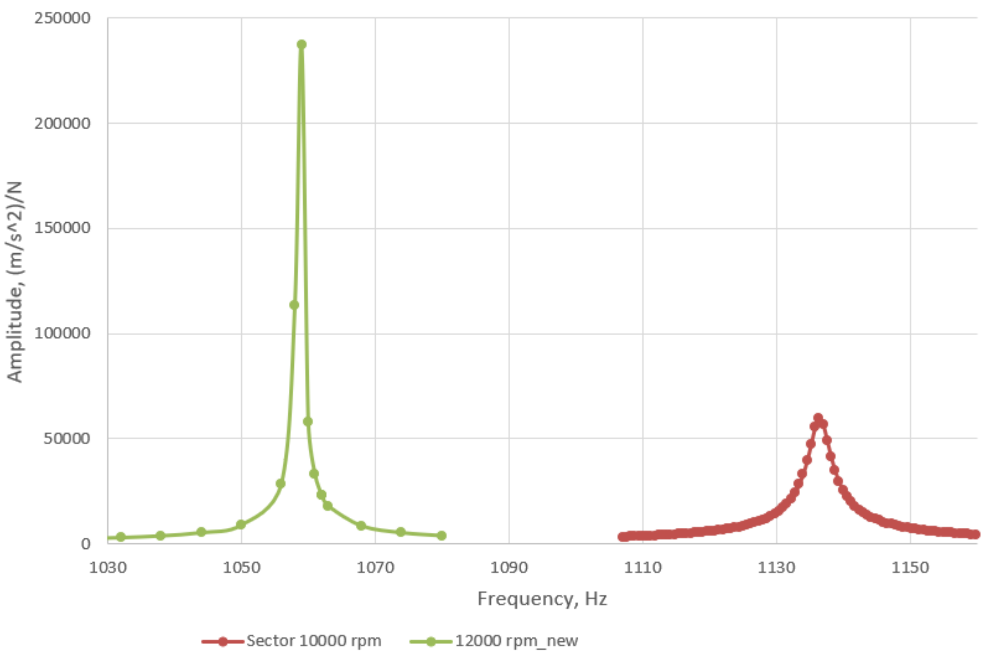

Figure 78: Comparison, bladed disk (green line) and sector of the disk (red line)

Future development The script presented in this thesis is tested comparing the numerical and experimental data for the dummy blade model. The relevancy between the numerical and experimental results is satisfactory. After this conclusion the script is tested for a real model of blade and the numerical calculations performed. In the last part of the thesis the real model of the blade is transformed in a complete bladed disk. Continuing the development of this thesis some improvements can be done:

1. test the model using an high-performance calculator
2. develop a misturing bladed disk changing the material properties and contact pressure of the blades

6 Appendix

	Amplitude				Amplitude		
Frequency	**F=50kN**	**F=45kN**	**F=25kN**	**Frequency**	**F=10kN**	**F=5kN**	**F=2kN**
185,25	9,00741	9,008357	9,019059	186,62	16,4796	16,4895	16,49899
185,5	9,85415	9,8551	9,86787	186,75	17,82557	17,83713	17,84829
185,75	10,8703	10,87167	10,88693	186,88	19,403	19,41665	19,42961
186	12,1126	12,11419	12,13304	187	21,27341	21,2897	21,30516
186,25	13,6647	13,66676	13,69045	187,12	23,52732	23,54709	23,56602
186,5	15,6577	15,66021	15,69096	187,25	26,29426	26,31876	26,34216
186,75	18,3065	18,30994	18,35138	187,38	29,75842	29,78934	29,81914
187	21,9892	21,99418	22,05299	187,5	34,19776	34,23815	34,27715
187,25	27,4289	27,43638	27,52594	187,62	40,0531	40,10729	40,15968
187,5	36,1608	36,17346	36,32349	187,75	48,01829	48,09358	48,16761
187,75	51,8061	51,82979	52,11257	187,88	59,12558	59,23261	32,58651
188	81,5238	81,56541	82,05991	188	74,49767	74,64348	35,79609
188,25	101,959	101,9414	101,7371	188,12	92,93514	93,08184	33,19079
188,5	69,4421	69,40701	68,99362	188,25	103,9149	103,9185	34,09583
188,75	45,5518	45,53367	45,32045	188,38	95,2246	95,08954	35,11423
189	33,0099	32,99987	32,88282	188,5	77,00112	76,85846	36,7779
189,25	25,712	25,70588	25,63392	188,62	61,14526	61,03922	39,00263
189,5	21,0143	21,01016	20,9621	188,75	49,60431	49,52949	49,44833
189,75	17,7576	17,75457	17,72045	188,88	41,33623	41,28243	41,23131
190	15,3739	15,37175	15,34624	189	35,26932	35,22941	35,19175
190,25	13,5565	13,55477	13,53519	189,12	30,68473	30,65438	30,62571
190,5	12,1262	12,12493	12,10931	189,25	27,12407	27,10031	27,07783
190,75	10,972	10,97099	10,95835	189,38	24,28738	24,26841	24,25029
191	10,0213	10,02042	10,00991	189,5	21,9773	21,9617	21,94696

Table 2: Data dummy blade, f=0.15

	Amplitude					
Frequency	**F=50kN**	**F=45kN**	**F=25kN**	**F=10kN**	**F=5kN**	**F=1kN**
186,62	16,3869	16,39367	16,42378	16,45953	16,47245	16,4862
186,75	17,7189	17,72671	17,76168	17,80313	17,81827	17,83424
186,88	19,2785	19,28774	19,32883	19,37764	19,39542	19,41417
187	21,1262	21,13729	21,18616	21,24428	21,26554	21,28804
187,12	23,3505	23,36393	23,4231	23,49345	23,5193	23,54612
187,25	26,0779	26,09438	26,16747	26,25426	26,28623	26,31987
187,38	29,4874	29,50823	29,6004	29,71005	29,75038	29,79308
187,5	33,8497	33,87646	33,99596	34,13808	34,19027	34,24592
187,62	39,592	39,62785	39,78711	39,97666	40,04656	40,12077
187,75	47,388	47,43729	47,65619	47,91698	48,01356	48,11751
187,88	58,2461	58,3151	58,62182	58,98762	59,12349	31,67777
188	73,3109	73,40429	73,8187	74,31167	74,49544	37,90987
188,12	91,7106	91,8074	92,23393	92,7348	92,91949	33,5268
188,25	103,699	103,7161	103,7829	103,8452	103,8599	32,42328
188,38	96,1826	96,09992	95,73021	95,28652	95,11854	33,41864
188,5	78,0892	77,99413	77,57443	77,08108	76,89886	35,99082
188,62	61,9678	61,89515	61,57547	61,202	61,06422	38,03968
188,75	50,1848	50,13315	49,90544	49,63891	49,54186	49,43356
188,88	41,7505	41,71313	41,54905	41,3568	41,28694	41,21356
189	35,5734	35,54572	35,42402	35,2813	35,22941	35,17511
189,12	30,9146	30,89357	30,80052	30,69137	30,65183	30,61032
189,25	27,3025	27,28596	27,21286	27,12718	27,09607	27,06355
189,38	24,429	24,41566	24,35704	24,28823	24,26331	24,23712
189,5	22,0917	22,08093	22,03287	21,97659	21,95603	21,93477

Table 3: Data dummy blade, f=0.30

	Amplitude					Amplitude		Amplitude	
Frequency	**F=50kN**	**F=25kN**	**F=10kN**	**F=5kN**	**Frequency**	**F=45kN**	**Frequency**	**F=1kN**	**F=0,6kN**
185,25	8,41793	8,427823	8,436359	8,441236	181	3,463339	186,5	14,09344	14,0941303
185,5	9,15821	9,169756	9,179673	9,185378	182	4,041133	187	19,08625	19,0865282
185,75	10,0361	10,0499	10,06175	10,06857	183	4,832646	187,5	29,19253	29,1919766
186	11,0939	11,11061	11,12495	11,13314	184	5,98334	188	57,63879	30,9582196
186,25	12,3927	12,41328	12,43108	12,44122	185	7,807749	188,5	69,23349	34,4156612
186,5	14,0246	14,0506	14,07298	14,08589	186	11,13724	189	41,46084	41,4525164
186,75	16,1343	16,16828	16,19774	16,21454	186,5	14,02726	189,5	24,25636	24,2549427
187	18,9634	19,00977	19,04981	19,07272	187	18,96822	190	17,03393	17,0333573
187,25	22,9436	23,01035	23,06793	23,10088	187,5	28,92869			
187,5	28,9179	29,02126	29,11051	29,162	188	56,7656			
187,75	38,7217	38,8993	39,05308	39,14172	188,5	96,46578			
188	56,7292	57,07006	57,36545	57,53651	189	41,94581			
188,25	89,4632	89,96112	90,38629	90,63112	189,5	24,42832			
188,5	96,5143	96,11495	95,76538	95,55749	190	17,11801			
188,75	62,538	62,16277	61,84406	61,66066	191	10,68421			
189	41,9661	41,77348	41,60933	41,51612	192	7,809605			
189,25	30,9855	30,87681	30,78406	30,73132	193	6,174321			
189,5	24,4356	24,36722	24,30896	24,27578	194	5,119952			
189,75	20,14	20,09352	20,054	20,0314	195	4,383857			
190	17,1214	17,08808	17,05958	17,04333	196	3,840948			
190,25	14,89	14,86495	14,84337	14,83123	197	3,42413			
190,5	13,1754	13,15589	13,13927	13,12981	198	3,094031			
190,75	11,8179	11,8024	11,78904	11,78143	199	2,826131			
191	10,7169	10,70423	10,69343	10,68724	200	2,60447			

Table 4: Data dummy blade, f=0.50

	Amplitude					Amplitude		Amplitude	
Frequency	**F=50kN**	**F=25kN**	**F=10kN**	**F=5kN**	**Frequency**	**F=45kN**	**Frequency**	**F=1kN**	**F=0,6kN**
185,25	8,4178	8,428907	8,437578	8,439881	181	3,463339	186,5	14,0955	14,0945423
185,5	9,15794	9,171114	9,181167	9,183748	182	4,041133	187	19,08984	19,0880467
185,75	10,0359	10,0514	10,06339	10,06666	183	4,832646	187,5	29,20044	29,1966955
186	11,0937	11,11252	11,127	11,13082	184	5,98334	188	57,65958	29,1176461
186,25	12,3923	12,41561	12,43355	12,43834	185	7,807749	188,5	95,40178	32,3468751
186,5	14,0241	14,05349	14,07614	14,08218	186	11,13724	189	41,44702	41,4519523
186,75	16,1336	16,17213	16,20173	16,20972	186,5	14,02726	189,5	24,25126	24,2538086
187	18,9624	19,01502	19,05533	19,06623	187	18,96822	190	17,03136	17,0326447
187,25	22,9422	23,01769	23,07582	23,09147	187,5	28,92869			
187,5	28,9156	29,03278	29,123	29,14742	188	56,7656			
187,75	38,7178	38,91907	39,07395	39,1164	188,5	96,46578			
188	56,7215	57,10759	57,40563	57,48698	189	41,94581			
188,25	89,4513	90,01512	90,44253	90,55991	189,5	24,42832			
188,5	96,5253	96,07427	95,72259	95,62132	190	17,11801			
188,75	62,5463	62,12184	61,7999	61,71298	191	10,68421			
189	41,9703	41,75233	41,58691	41,54263	192	7,809605			
189,25	30,9879	30,86493	30,77133	30,7463	193	6,174321			
189,5	24,437	24,35971	24,30102	24,28528	194	5,119952			
189,75	20,1409	20,0884	20,04846	20,0378	195	4,383857			
190	17,1221	17,08452	17,05573	17,04804	196	3,840948			
190,25	14,8905	14,86209	14,84052	14,83466	197	3,42413			
190,5	13,1758	13,15374	13,13697	13,13239	198	3,094031			
190,75	11,8182	11,80068	11,78718	11,78358	199	2,826131			
191	10,7172	10,70294	10,69199	10,68911	200	2,60447			

Table 5: Data dummy blade, f=0.70

		Amplitude			
Frequency	**15000rpm**	**10000rpm**	**5000rpm**	**3000rpm**	**2000rpm**
1120,3	5895,51	6018,919	6136,973	6179,104	1309,124
1120,6	6007,08	6135,204	6257,882	6301,706	1310,297
1120,9	6122,83	6255,955	6383,525	6429,143	1311,326
1121,2	6243,03	6381,424	6514,183	6561,712	1312,593
1121,5	6367,9	6511,9	6650,163	6699,718	1313,614
1121,8	6497,74	6647,68	6791,79	6843,512	1314,585
1122,1	6632,84	6789,095	6939,431	6993,458	1315,815
1122,4	6773,53	6936,497	7093,468	7149,956	1316,643
1122,7	6920,17	7090,279	7254,321	7313,446	1317,447
1123	7073,13	7250,854	7422,452	7484,402	1318,574
1123,3	7232,83	7418,687	7598,371	7663,348	1319,562
1123,6	7399,71	7594,271	7782,609	7850,84	1320,208
1123,9	7574,28	7778,153	7975,782	8047,521	1321,067
1124,2	7757,07	7970,925	8178,538	8254,072	1321,927
1124,5	7948,67	8173,249	8391,611	8471,244	1322,763
1124,8	8149,72	8385,845	8615,801	8699,887	1323,598
1125,1	8360,95	8609,504	8851,986	9212,082	1324,414
1125,4	8583,12	8845,107	9101,149	9190,04	1325,221
1125,7	8817,11	9093,621	9364,377	3341,438	1326,013
1126	9063,87	9356,125	9642,878	3337,013	1326,794
1126,3	9324,47	9633,824	9938,007	3334,594	1327,497
1126,6	9600,08	9928,05	10251,28	3331,731	1328,209
1126,9	9892,02	10240,31	10584,39	3327,931	1328,976
1127,2	10201,8	10572,27	10939,31	3322,65	1330,095
1127,5	10531	10925,85	11318,12	3318,507	1330,783
1127,8	10881,5	11303,16	11723,31	3313,886	1331,462
1128,1	11255,4	11706,66	12157,69	3309,294	1332,11
1128,4	11655,2	12139,09	12624,47	3305,208	1332,693
1128,7	12083,4	12603,61	13127,31	3298,436	1333,286
1129	12543,3	13103,85	13670,45	3295,364	1333,678
1129,3	13038,3	13644,01	14258,84	3287,529	1333,908
1129,6	13572,4	14228,81	14898,19	3282,788	1334,486
1129,9	14150,5	14863,89	15595,16	3277,37	1335,013
1130,2	14778	15555,78	16357,57	3270,442	1335,546
1130,5	15461,1	16312,11	17194,82	3266,144	1336,043
1130,8	16207,5	17141,93	18117,97	3259,129	1336,515
1131,1	17025,7	18055,91	19140,22	3260,859	1336,967
1131,4	17926,2	19066,74	20277,49	3247,459	1337,403
1131,7	18921,3	20189,54	21549,37	3240,055	1337,829
1132	20025,5	21442,58	22979,39	3233,415	1338,22
1132,3	21256,5	22847,62	13004,31	3224,966	1338,626
1132,6	22635,2	24430,6	12882,07	3218,278	1338,986
1132,9	24186,7	26222,34	12756,24	3212,414	1339,325
1133,2	25940,6	28259,56	12617,96	3203,165	1339,634
1133,5	27932,1	30584,41	12484,8	3195,503	1339,324
1133,8	30201,7	33242,55	12343,21	3188,06	1339,312

1134,1	32794,1	36277,89	12201,42	3181,943	1340,362
1134,4	35753	39719,8	12052,55	3173,272	1340,603
1134,7	39110,6	43558,34	11898,07	3163,951	1340,784
1135	42866,9	47692,16	11743,98	3156,933	1879,307
1135,3	46946,3	51861,04	11587,37	3148,578	1341,505
1135,6	51133,7	55584,18	11429,04	3140,081	1341,323
1135,9	55010,2	58219,46	11291,74	3125,032	1341,64
1136,2	57964,3	59194,94	12179,85	3123,116	1341,976
1136,5	59373,6	58322,55	11975,93	3114,577	1866,078
1136,8	58913	55902,95	12741,26	3105,834	1342,374
1137,1	56754,8	52465,1	18632,97	3667,024	1342,056
1137,4	53417,6	48573,76	21134,25	3087,147	1342,152
1137,7	49504,7	44638,7	22152,72	3078,209	1342,216
1138	45485,7	40908,85	21148,43	3069,264	1341,728
1138,3	41650,8	37500,52	20227,05	3059,512	1342,404
1138,6	38138,8	34449,78	19358,33	3050,832	1342,385
1138,9	34995,5	31748,21	18540,6	3040,57	1342,376
1139,2	32214,6	29365,47	19867,26	3030,89	1342,315
1139,5	29765,7	27264,98	22451,95	3021,779	1342,294
1139,8	27610,4	25409,98	23583,14	3011,912	1342,221
1140,1	25710	23767,01	22155,63	3001,495	1342,097
1140,4	24029,2	22306,25	20875,79	2993,012	1341,976
1140,7	22537	21001,92	19725,11	2983,26	1341,83
1141	21206,3	19832,33	18686,94	2972,438	1341,934
1141,3	20014,4	18779,25	17746,91	4276,659	1341,72
1141,6	18959,5	17827,21	16892,58	4245,872	1341,494
1141,9	17988,4	16980,09	16113,48	4213,228	1341,216
1142,2	17108,1	16190,23	15400,67	4183,447	1340,926
1142,5	16307	15468,47	14746,33	4150,949	1340,915
1142,8	15575,5	14806,66	14143,82	6295,854	1340,325
1143,1	14905	14197,87	13601,44	7794,3	1340,064
1143,4	14288,6	13636,18	13084,37	7643,456	1339,792
1143,7	13720,2	13116,49	12604,55	7805,242	1339,545
1144	13194,5	12634,36	12158,21	9171,254	1339,173
1144,3		12185,96	11742,05	10005,79	1338,811
1144,6		11767,96	11353,15	9732,089	1780,802
1144,9		11377,42	10988,97	9886,754	1777,316
1145,2		11011,77	10647,29	9893,825	1773,888
1145,5		10668,76	10326,1	9475,1	1337,238
1145,8		10346,36	10023,65	9586,698	1336,72
1146,1		10042,81	9738,369	9327,26	1336,419
1146,4		9756,527	9468,852	9081,425	1757,466
1146,7		9486,091	9213,844	8846,044	1754,301
1147		9230,248	8972,224	8881,301	1751,874
1147,3		8987,851	8742,975	8661,067	1748,415
1147,6		8757,889	8525,181	8447,312	1333,442
1147,9		8539,434	8318,007	8243,884	1333,109

1148,2		8331,651	8120,71	8050,072	1738,507
1148,5		8133,791	7932,608	7865,209	1734,156
1148,8		7945,157	7753,075	7688,699	1732,014
1149,1		7765,132	7581,546	7519,992	1727,701
1149,4		7593,135	7417,496		1724,06
1149,7		7428,658	7260,457		1721,261
1150		7271,211	7109,986		1716,786

Table 6: Data section of the disk, f=0.15

Frequency	**Amplitude 15000rpm**	**Frequency**	**Amplitude 10000rpm**	**Frequency**	**Amplitude 5000rpm**
1121,78	6401,188	1107	3217,475	1120	5943,939
1122,15	6565,862	1107,6	3286,694	1120,4	6096,193
1122,53	6739,131	1108,2	3358,841	1120,8	6256,237
1122,9	6921,418	1108,8	3434,095	1121,2	6424,689
1123,28	7113,706	1109,4	3512,663	1121,6	6602,212
1123,65	7316,562	1110	3594,771	1122	6789,565
1124,03	7531,162	1110,6	3680,659	1122,4	6987,574
1124,4	7758,248	1111,2	3770,592	1122,8	7197,168
1124,78	7999,234	1111,8	3864,871	1123,2	7419,398
1125,15	8255,124	1112,4	3963,811	1123,6	7655,42
1125,53	8527,63	1113	4067,771	1124	7906,557
1125,9	8818,092	1113,6	4177,137	1124,4	8174,286
1126,28	9128,654	1114,2	4292,338	1124,8	8460,296
1126,65	9461,099	1114,8	4413,865	1125,2	8766,5
1127,03	9818,154	1115,4	4542,237	1125,6	9095,091
1127,4	10202,23	1116	4678,061	1126	9448,589
1127,78	10616,87	1116,6	4821,991	1126,4	9829,896
1128,15	11065,38	1117,2	4974,781	1126,8	10242,36
1128,53	11552,43	1117,8	5137,268	1127,2	10689,92
1128,9	12082,64	1118,4	5310,406	1127,6	11177,15
1129,28	12662,35	1119	5495,267	1128	11709,48
1129,65	13298,13	1119,6	5693,079	1128,4	12293,3
1130,03	13998,8	1120,2	5905,247	1128,8	12936,28
1130,4	14773,89	1120,8	6133,387	1129,2	13647,67
1130,78	15636,06	1121,4	6379,361	1129,6	14438,65
1131,15	16599,53	1122	6645,324	1130	15322,82
1131,53	17682,93	1122,6	6933,81	1130,4	16316,96
1131,9	18908,03	1123,2	7247,774	1130,8	17441,96
1132,28	20303,21	1123,8	7590,727	1131,2	18723,95
1132,65	21902,41	1124,4	7966,833	1131,6	20195,91
1133,03	23749,57	1125	8381,098	1132	21899,58
1133,4	25897,82	1125,6	8839,563	1132,4	23888,3
1133,78	28414,34	1126,2	9349,615	1132,8	26229,97

1134,15	31376,77	1126,8	9920,337	1133,2	29009,51
1134,53	34871,76	1127,4	10563,06	1133,6	32329,13
1134,9	38971,02	1128	11292,03	1134	36297,37
1135,28	43685,27	1128,6	12125,48	1134,33	40157,5
1135,65	48848,73	1129,2	13086,95	1134,4	40990,46
1136,03	53940,31	1129,8	14207,43	1134,67	44503,96
1136,4	57947,09	1130,4	15528,35	1134,8	46349,14
1136,78	59644,24	1131	17106,03	1135	39141,65
1137,15	58410,33	1131,6	19018,62	1135,17	38583,95
1137,53	54772,25	1132,2	21376,04	1135,18	38545,51
1137,9	49897,79	1132,8	24335,21	1135,26	38357,2
1138,28	44811,24	1133,4	28119,37	1135,42	38289,98
1138,65	40079,58	1134	33031,84	1135,58	36924,12
1139,03	35916,17	1134,6	39406,33	1135,6	41405,59
1139,4	32339,65	1135,2	47280,36	1135,74	42682,03
1139,78	29294,52	1135,8	55301,6	1135,82	37864,63
1140,15	26728,9	1136,4	59494,5	1135,83	37796,77
1140,53	24505,58	1137	56646,48	1135,9	40716,5
1140,9	22594,65	1137,6	49251,46	1136,17	39310,55
1141,28	20941,61	1138,2	41370,05	1136,33	41003,98
1141,65	19500,86	1138,8	34746,9	1136,33	41003,98
1142,03	18237,1	1139,4	29559,76	1136,4	40558,38
1142,4	17120,77	1140	25541,81	1136,5	39954,46
1142,78	16129,15	1140,6	22420,73	1136,67	41795,91
1143,15	15242,78	1141,2	19914,45	1136,67	41795,91
1143,53	14446,77	1141,8	17888,49	1136,8	40736,75
1143,9	13727,93	1142,4	16223,29	1136,83	40478,54
1144,28	13076,29	1143	14833,9	1137	42079,43
1144,65	12482,66	1143,6	13659,08	1137	42079,43
1145,03	11940,19	1144,2	12653,91	1137,2	43244,86
1145,4	11442,29	1144,8	11784,89	1137,33	44882,08
1145,78	10984,13	1145,4	11026,6	1137,6	44578,74
1146,15	10560,88	1146	10359,49	1137,67	43740,24
1146,53	10169,09	1146,6	9768,257	1138	39700,74
1146,9	9805,093	1147,2	9240,808	1138	39700,74
1147,28	9466,387	1147,8	8767,464	1138,4	35403,31
1147,65	9150,159	1148,4	8340,385	1138,8	31729,12
1148,03	8854,557	1149	7953,167	1139,2	28618,47
1148,4	8577,364	1149,6	7600,515	1139,6	25986,51
1148,78	8317,204	1150,2	7278,044	1140	23750,72
1149,15	8072,303	1150,8	6982,048	1140,4	21839,14
1149,53	7841,626	1151,4	6709,43	1140,8	20192,92
1149,9	7623,724	1152	6457,535	1141,2	18764,58
1150,28	7417,826	1152,6	6224,095	1141,6	17532,44
1150,65	7222,726	1153,2	6007,168	1142	16430,28
1151,03	7037,844	1153,8	5805,069	1142,4	15454,45
1151,4	6862,167	1154,4	5616,333	1142,8	14585,23

		1155	5439,683	1143,2	13806,57
		1155,6	5274,001	1143,6	13105,42
		1156,2	5118,295	1144	12471,03
		1156,8	4971,692	1144,4	11894,52
		1157,4	4833,423	1144,8	11368,46
		1158	4702,801	1145,2	10886,64
		1158,6	4579,207	1145,6	10443,78
		1159,2	4462,087	1146	10035,42
		1159,8	4350,952	1146,4	9657,715
		1160,4	4245,352	1146,8	9307,401
		1161	4144,886	1147,2	8981,629
		1161,6	4049,185	1147,6	8677,935
		1162,2	3957,931	1148	8394,175
		1162,8	3870,804	1148,4	8128,46
		1163,4	3787,548	1148,8	7879,145
		1164	3707,895	1149,2	7644,763
		1164,6	3631,627	1149,6	7424,027
		1165,2	3558,535	1150	7215,785
		1165,8	3488,415	1150,4	7019,014
		1166,4	3421,093	1150,8	6832,796
Frequency	**Amplitude 3000rpm**	**Frequency**	**Amplitude 2000rpm**		
1120,3	6101,764	1122,4	7066,398		
1120,6	6221,29	1123,4	7627,445		
1120,9	6345,466	1124,4	8282,654		
1121,2	6474,565	1125,4	3720,345		
1121,5	6608,895	1126,4	3705,837		
1121,8	6748,766	1127,4	3686,438		
1122,1	6894,535	1128,4	3660,327		
1122,4	7046,574	1129,4	3635,188		
1122,7	7205,296	1130,4	3604,94		
1123	7371,156	1131,4	3572,196		
1123,3	7544,626	1131,73	3560,911		
1123,6	7726,254	1132,07	3549,891		
1123,9	7916,619	1132,4	3536,921		
1124,2	8116,355	1132,73	3525,767		
1124,5	8326,17	1133,07	3513,424		
1124,8	8546,839	1133,4	3501,473		
1125,1	8779,219	1133,73	3487,28		
1125,4	9024,254	1134,07	3475,287		
1125,7	9282,998	1134,4	3459,671		
1126	9556,615	1134,73	3447,787		
1126,3	9846,415	1135,07	3433,531		
1126,6	10153,85	1135,4	3420,25		
1126,9	10480,54	1135,73	3408,204		
1127,2	10828,34	1136,07	3393,186		
1127,5	11199,33	1136,4	3380,342		

1127,8	11595,86	1136,73	3366,798
1128,1	12020,6	1137,07	3350,712
1128,4	12476,67	1137,4	3336,483
1128,7	12967,45	1137,73	3323,487
1129	13497,06	1138,07	3306,933
1129,3	14070,17	1138,4	3293,656
1129,6	14692,17	1138,73	3279,85
1129,9	15369,41	1139,07	3265,986
1130,2	16109,3	1139,4	3250,632
1130,5	16920,6	1139,73	3236,387
1130,8	17813,82	1140,07	3221,765
1131,1	18801,56	1140,4	3206,508
1131,4	8744,264	1140,73	3191,709
1131,7	8691,606	1141,07	3177,204
1132	8636,343	1141,4	3161,262
1132,3	8581,62	1142,4	3117,724
1132,6	8522,46	1143,4	3072,826
1132,9	8459,509	1144,4	3028,517
1133,2	8399,799	1145,4	7961,924
1133,5	8331,44	1146,4	7701,222
1133,8	8270,688	1147,4	7607,289
1134,1	8196,448	1148,4	8024,918
1134,4	7036,139	1149,4	7445,665
1134,7	8067,938	1150,4	6943,366
1135	7997,353	1151,4	6505,168
1135,3	7928,227		
1135,6	7857,589		
1135,9	7785,14		
1136,2	7710,992		
1136,5	7641,825		
1136,8	7568,021		
1137,1	7496,035		
1137,4	7421,978		
1137,7	7349,03		
1138	7278,129		
1138,3	8003,094		
1138,6	15927,32		
1138,9	15383,29		
1139,2	15585,34		
1139,5	15029,43		
1139,8	14508,59		
1140,1	14598,76		
1140,4	14090,01		
1140,7	13617,99		
1141	18958,95		
1141,3	18042,22		
1141,6	17159,93		

1141,9	16356,38
1142,2	15639,64
1142,5	14963,7
1142,8	14342,39
1143,1	13769,54
1143,4	13239,87
1143,7	12748,8
1144	12292,36
1144,3	11867,11
1144,6	11470
1144,9	11098,4
1145,2	10749,96
1145,5	10422,62
1145,8	10114,55
1146,1	9824,125
1146,4	9549,884
1146,7	9290,537
1147	9044,906
1147,3	8811,954
1147,6	8590,728
1147,9	8380,384
1148,2	8180,132
1148,5	7989,281
1148,8	7807,182
1149,1	7633,252
1149,4	7466,965
1149,7	7307,828
1150	7155,388

Table 7: Data section of the disk, f=0.30

			Amplitude		
Frequency	**15000rpm**	**10000rpm**	**5000rpm**	**3000rpm**	**2000rpm**
1120,3	5824,44	5941,917	6057,047	6174,293	6192,224
1120,6	5933,34	6055,245	6174,804	6296,639	6315,289
1120,9	6046,28	6172,863	6297,104	6423,806	6443,215
1121,2	6163,48	6295,016	6424,223	6556,074	6576,288
1121,5	6285,19	6421,971	6556,44	6693,759	6714,828
1121,8	6411,68	6554,016	6694,072	6837,203	6859,187
1122,1	6543,23	6691,459	6837,45	6986,767	7009,722
1122,4	6680,14	6834,642	6986,943	7142,844	7166,836
1122,7	6822,76	6983,921	7142,946	7305,878	7330,977
1123	6971,43	7139,694	7305,894	7476,331	7502,614
1123,3	7126,56	7302,396	7476,257	7654,72	7682,272
1123,6	7288,57	7472,49	7654,543	7841,605	7870,517
1123,9	7457,92	7650,488	7841,32	8037,607	8067,981
1124,2	7635,12	7836,945	8037,194	8243,4	8275,357

1124,5	7820,73	8032,483	8242,853	8459,727	8493,389
1124,8	8015,34	8237,767	8459,027	8687,415	8722,913
1125,1	8219,63	8453,54	8686,543	8927,367	8964,857
1125,4	8434,32	8680,616	8926,308	9180,59	9220,24
1125,7	8660,24	8919,897	9179,322	9448,203	9490,21
1126	8898,26	9172,383	9446,697	9731,448	9776,016
1126,3	9149,37	9439,176	9729,678	10031,72	10079,09
1126,6	9414,67	9721,523	10029,65	10350,57	10401,02
1126,9	9695,39	10020,79	10348,17	10689,76	10743,58
1127,2	9992,87	10338,53	10686,98	11051,25	11108,8
1127,5	10308,7	10676,47	11048,03	11437,28	11498,94
1127,8	10644,4	11036,57	11433,56	11850,38	11916,59
1128,1	11002,2	11421,03	11846,09	12293,43	12364,73
1128,4	11384	11832,36	12288,48	12769,72	12846,72
1128,7	11792,4	12273,41	12764,03	13283,05	13366,4
1129	12230,3	12747,43	13276,48	13837,77	13928,33
1129,3	12700,7	13258,17	13830,2	14438,95	14537,64
1129,6	13207,4	13809,93	14430,18	15092,45	15200,48
1129,9	13754,6	14407,69	15082,28	15805,13	15923,77
1130,2	14347,3	15057,22	15793,31	16585,01	16715,96
1130,5	14991	15765,28	16571,25	17441,69	17586,84
1130,8	15692,5	16539,79	17425,53	18386,28	7048,121
1131,1	16459,4	17390,05	18367,28	19432,21	7016,587
1131,4	17301	18327,09	19409,76	20595,46	6984,803
1131,7	18228,1	19363,99	20568,82	21895,15	6950,935
1132	19253,4	20516,36	21863,18	23354,14	9564,446
1132,3	20392,2	21802,75	23315,51	24999,65	10013,36
1132,6	21662,8	23245,47	24952,75	26864,03	6848,982
1132,9	23086,8	24871,05	26806,82	28985,27	6811,757
1133,2	24690,4	26710,99	28915,03	31406,29	10764,78
1133,5	26504,1	28801,8	31319,47	34172,61	9403,83
1133,8	28564,1	31185	34064,53	37325,57	11009,81
1134,1	30911,2	33904,41	37190,36	40888,95	7796,909
1134,4	33588,8	37000,35	40718,58	37598,24	10714,56
1134,7	36638,2	40495,9	44622,53	36652,6	10571,76
1135	40085,6	44369,8	48779,34	35572,4	10420,02
1135,3	43917,1	48510,84	52901,72	31101,9	10274,75
1135,6	48035,8	52651,3	56490,37	33467,84	10129,83
1135,9	52198,3	56315,96	58895,99	34111,75	9987,654
1136,2	55957,7	58864,18	59564,31	34572,53	9840,48
1136,5	58687,4	59712,17	58347,32	35159,95	9702,513
1136,8	59775,9	58650,55	55583,5	31379,22	9554,861
1137,1	58947,7	55973,94	51878,61	35055,98	9420,29
1137,4	56435,5	52286,84	47815,1	37343,47	9279,368
1137,7	52825,3	48196,8	43801,77	39830,03	9154,267
1138	48742,8	44137,73	40061,41	36503,34	9033,473
1138,3	44650,7	40348,44	36685,63	33542,19	13234,52

1138,6	40810,7	36928,11	33689,42	30929,61	12874,88
1138,9	37372,6	33893,83	31050,15	28630,77	12529,48
1139,2	34278,4	31252,8	28730,69	26606,45	15842,54
1139,5	31555,9	28900,92	26690,35	24819,45	16133,99
1139,8	29166,9	26834,8	24914,74	23236,38	15519,75
1140,1	27069	25014,58	23316,42	21828,13	17535,74
1140,4	25221,5	23404,7	21896,08	20589,26	17344,03
1140,7	23588,5	21974,66	20628,2	19456,38	17547,55
1141	22138,6	20698,57	19491,34	18435,89	18263,96
1141,3	20845,6	19554,7	18467,47	17512,79	17374,94
1141,6	19687,2	18524,83	17541,48	16674,45	16549,2
1141,9	18644,8	17593,67	16700,65	15910,23	15795,98
1142,2	17702,7	16748,37	15934,27	15211,09	15106,47
1142,5	16847,9	15978,08	15233,25	14569,35	14473,23
1142,8	16069,3	15273,62	14589,85	13978,43	13889,87
1143,1	15357,6	14627,2	13997,48	13432,71	13350,82
1143,4	14704,7	14032,15	13450,47	12927,32	12851,42
1143,7	14103,8	13482,75	12943,94	12458,06	12387,51
1144	13549,3	12974,08	12473,66	12021,28	11955,55
1144,3		12501,88	12035,96	11613,79	11552,41
1144,6		12062,45	11627,64	11232,79	11175,33
1144,9		11652,57	11245,89	10875,83	10821,95
1145,2		11269,4	10888,25	10540,74	10490,11
1145,5		10910,46	10552,53	10225,6	10177,92
1145,8		10573,57	10236,82	9928,706	9883,743
1146,1		10256,78	9939,402	9648,538	9606,067
1146,4		9958,361	9658,752	9383,737	9343,558
1146,7		9676,796	9393,508	9133,096	9095,025
1147		9410,707	9142,451	8895,511	8859,393
1147,3		9158,875	8904,489	8670,011	8635,693
1147,6		8920,189	8678,632	8455,698	8423,052
1147,9		8693,657	8463,99	8251,765	8220,673
1148,2		8478,387	8259,748	8057,494	8027,843
1148,5		8273,569	8065,184	7872,208	7843,905
1148,8		8078,458	7879,634	7695,31	7668,265
1149,1		7892,399	7702,479	7526,248	7500,376
1149,4		7714,768	7533,177	7364,516	7339,742
1149,7		7545,021	7371,22		7185,903
1150		7382,638	7216,135		7038,442

Table 8: Data section of the disk, f=0.70

Frequency	Amplitude 12000rpm
1026	2238,569
1032	2766,395
1038	3600,722
1044	5117,631
1050	8734,317
1056	28608,89
1058	113235,6
1059	237006,8
1060	58028,86
1061	33102,13
1062	23127,64
1062	23175,17
1063	17840,19
1068	8325,241
1074	5109,598
1080	3703,057

Table 9: Data bladed disk, f=0.70, blade 1

Frequency	Amplitude 12000rpm
1026	2238,569
1032	2766,395
1038	3600,722
1044	5117,631
1050	8734,317
1056	28608,89
1062	23127,64
1068	8325,241
1074	5109,598
1080	3703,057
1058	113235,6
1059	237006,8
1060	58028,86
1061	33102,13
1062	23175,17

Table 10: Data bladed disk, f=0.70, blade 45

Frequency	Amplitude 12000rpm
1026	2238,569
1032	2766,395
1038	3600,722
1044	5117,631
1050	8734,317
1056	28608,89
1062	23127,64
1068	8325,241
1074	5109,598
1080	3703,057
1058	113235,6
1059	237006,8
1060	58028,86
1061	33102,13
1062	23175,17
1063	17840,19

Table 11: Data bladed disk, f=0.70, blade 73

List of Figures

List of Tables

References

[1] R. S. Abhari and M. Giles. A Navier–Stokes Analysis of Airfoils in Oscillating Transonic Cascades for the Prediction of Aerodynamic Damping. *Journal of Turbomachinery*, 119(1):77–84, 01 1997.

[2] Marco Allarà. A model for the characterization of friction contacts in turbine blades. *Journal of Sound and Vibration - J SOUND VIB*, 320:527–544, 02 2009.

[3] Daniele Botto, Chiara Gastaldi, Muzio Gola, and Muhammad Umer. An experimental investigation of the dynamics of a blade with two under-platform dampers. *Journal of Engineering for Gas Turbines and Power*, 140, 09 2017.

[4] M Ciavarella, DA Hills, and G Monno. The influence of rounded edges on indentation by a flat punch. *Proceedings of the Institution of Mechanical Engineers, Part C: Journal of Mechanical Engineering Science*, 212(4):319–327, 1998.

[5] Charleux D, C. Gibert, Fabrice Thouverez, and Dupeux J. Numerical and experimental study of friction damping blade attachments of rotating bladed disks. *International Journal of Rotating Machinery*, 2006, 07 2006.

[6] LE Goodman and JH Klumpp. Analysis of slip damping with reference to turbine blade vibration. *Journal of Applied Mechanics*, 23(2):421–429, 1956.

[7] IG Goryacheva, H Murthy, and TN Farris. Contact problem with partial slip for the inclined punch with rounded edges. *International journal of fatigue*, 24(11):1191–1201, 2002.

[8] MP Hanson. A vibration damper for axial flow compressor blading. *Proceedings Society Experimental Stress Analysis*, 14:155–162, 1955.

[9] KL Johnson. Contact mechanics cambridge univ. *Press, Cambridge*, 95:365, 1985.

[10] David IG Jones. Vibrations of a compressor blade with slip at the root. Technical report, AIR FORCE WRIGHT AERONAUTICAL LABS WRIGHT-PATTERSON AFB OH, 1980.

[11] JJ Kielb and Reza S Abhari. Experimental study of aerodynamic and structural damping in a full-scale rotating turbine. *J. Eng. Gas Turbines Power*, 125(1):102–112, 2003.

[12] Benjamin Joseph Lazan. Damping of materials and members in structural mechanics. *PERGAMON PRESS LTD, OXFORD, ENGLAND. 1968, 317*, 1968.

[13] SS Manson. Stress investigations in gas turbine discs and blades. Technical report, SAE Technical Paper, 1949.

[14] SS Manson, AJ Meyer, HF Calvert, and MP Hanson. Factors affecting vibration of axial flow compressor blades. *Proceedings of the society for experimental stress analysis*, 7(2), 1948.

[15] Shashikant T More and RS Bindu. Effect of mesh size on finite element analysis of plate structure. *Int. J. Eng. Sci. Innovative Technol*, 4(3):181–185, 2015.

[16] Christophe Pierre, AA Ferri, and EH Dowell. Multi-harmonic analysis of dry friction damped systems using an incremental harmonic balance method. 1985.

[17] H Poritsky. Stresses and deflections of cylindrical bodies in contact with application to contact of gears and of locomotive wheels. *J. appl. Mech.*, 17:191–201, 1950.

[18] JS Rao et al. Interface damping in attachment region. In *Proceedings of the 3rd International Conference on Rotordynamics, IFToMM, CNRS, Lyon*, pages 185–190, 1990.

[19] JS Rao, K Gupta, and N Vyas. Blade damping measurements in a spin rig with nozzle passing excitation simulated by electromagnets. *The Shock and vibration bulletin*, (56):II–109, 1986.

[20] Asmi Rizvi, Christopher Smith, Ramesh Rajasekaran, and Eric Ken. Dynamics of dry friction damping in gas turbines: Literature survey. *Journal of Vibration and Control*, 22, 01 2014.

[21] A Sackfield and DA Hills. Some useful results in the classical hertz contact problem. *The Journal of Strain Analysis for Engineering Design*, 18(2):101–105, 1983.

[22] KY Sanliturk, M Imregun, and DJ Ewins. Harmonic balance vibration analysis of turbine blades with friction dampers. 1997.

[23] James Forrest Shannon. *Vibration problems in gas turbines, centrifugal and axial flow compressors*. HM Stationery Office London, 1945.

[24] I Ya Shtaerman. Contact problem of the theory of elasticity. Technical report, FOREIGN TECHNOLOGY DIV WRIGHT-PATTERSON AFB OH, 1970.

[25] DA Spence. The hertz contact problem with finite friction. *Journal of elasticity*, 5(3-4):297–319, 1975.

[26] AV Srinivasan, DG Cutts, and S Sridhar. Turbojet engine blade damping. 1981.

[27] AV Srinivasan, DG Cutts, and S Sridhar. Turbojet engine blade damping. 1981.

[28] Aleksandr Mihaylovich Ulanov. Strength calculation of aircraft engines. *Publisher of the Samara University - ISBN : 978-5-7883-1364-1*, 320, 01 2017.

[29] Muhammad Umer and Daniele Botto. Measurement of contact parameters on underplatform dampers coupled with blade dynamics. *International Journal of Mechanical Sciences*, 159, 06 2019.

[30] Ying Wang, Francesco Dell'Isola, Tiejun Liu, and Chunhui Yang. Metamaterials and smart structures in a big data era. *Advances in Materials Science and Engineering*, 2017, 2017.

[31] JR Willis. Hertzian contact of anisotropic bodies. *Journal of the Mechanics and Physics of Solids*, 14(3):163–176, 1966.